EAG2 potassium channel with evolutionarily conserved function as a brain tumor target

Xi Huang[1,11,12], **Ye He**[1,11], **Adrian M. Dubuc**[2,11], **Rintaro Hashizume**[3], **Wei Zhang**[1], **Jüri Reimand**[4], **Huanghe Yang**[1], **Tongfei A. Wang**[1], **Samantha J. Stehbens**[5], **Susan Younger**[1], **Suzanne Barshow**[1], **Sijun Zhu**[1], **Michael K. Cooper**[6], **John Peacock**[2], **Vijay Ramaswamy**[2], **Livia Garzia**[2], **Xiaochong Wu**[2], **Marc Remke**[2], **Craig M. Forester**[7], **Charles C. Kim**[8], **William A. Weiss**[3], **C. David James**[3], **Marc A. Shuman**[9], **Gary D. Bader**[4], **Sabine Mueller**[10], **Michael D. Taylor**[2], **Yuh Nung Jan**[1,13], and **Lily Yeh Jan**[1,13]

[1]Howard Hughes Medical Institute, Departments of Physiology, Biophysics and Biochemistry, University of California, San Francisco, San Francisco, CA, 94143, USA

[2]Division of Neurosurgery, Arthur and Sonia Labatt Brain Tumor Research Centre, Hospital for Sick Children, Toronto, ON, M5G 0A4, Canada

[3]Department of Neurological Surgery and Helen Diller Family Comprehensive Cancer Center, University of California, San Francisco, San Francisco, CA, 94143, USA

[4]The Donnelly Centre, University of Toronto, Toronto, ON, M5S 3E1, Canada

[5]Department of Cell and Tissue Biology, University of California, San Francisco, San Francisco, CA, 94143, USA

[6]Department of Neurology, Vanderbilt University Medical Center, Nashville, TN, 37232, USA

[7]Department of Pediatrics, University of California, San Francisco, San Francisco, CA, 94143, USA

[8]Division of Experimental Medicine, Department of Medicine, UCSF, San Francisco, CA 94110, USA

[13]Authors for correspondence: Lily Yeh Jan, Ph.D. lily.jan@ucsf.edu Tel. 415-476-8748. Yuh Nung Jan, Ph.D. yuhnung.jan@ucsf.edu Tel. 415-476-8747.
[11]These authors contributed equally to this work.
[12]Current address:
Developmental & Stem Cell Program, Arthur and Sonia Labatt Brain Tumor Research Centre, Hospital for Sick Children, Toronto, ON, M5G 0A4, Canada
Department of Molecular Genetics, University of Toronto, Toronto, ON, M5S 1A8, Canada

[9]Department of Medicine and Helen Diller Family Comprehensive Cancer Center, University of California, San Francisco, San Francisco, CA, 94143, USA

[10]Department of Neurology and Helen Diller Family Comprehensive Cancer Center, University of California, San Francisco, San Francisco, CA, 94143, USA

Abstract

Over 20% of the drugs for treating human diseases target ion channels, however, no cancer drug approved by the U.S. Food and Drug Administration (FDA) is intended to target an ion channel. Here, we demonstrate the evolutionarily conserved function of EAG2 potassium channel in promoting brain tumor growth and metastasis, delineate downstream pathways and uncover a mechanism for different potassium channels to functionally corporate and regulate mitotic cell volume and tumor progression. We show that EAG2 potassium channel is enriched at the trailing edge of migrating MB cells to regulate local cell volume dynamics, thereby facilitating cell motility. We identify the FDA-approved antipsychotic drug thioridazine as an EAG2 channel blocker that reduces xenografted MB growth and metastasis, and present a case report of repurposing thioridazine for treating a human patient. Our findings thus illustrate the potential of targeting ion channels in cancer treatment.

Keywords

EAG potassium channel; medulloblastoma; brain tumor; metastasis; *Drosophila*

Medulloblastoma (MB), the most common malignant pediatric brain tumor, frequently metastasizes along the leptomeninges of the brain and spinal cord. MB is composed of four molecular and clinical subgroups (SHH, WNT, group 3 and group 4)[1–4]. SHH-MBs represent one-quarter of all MBs, and mouse mutants with constitutive activation of Shh pathway in the cerebella develop MBs that resemble human SHH-MBs[5–8]. SHH pathway inhibitors are in clinical trials for recurrent disease[9–11], however, growth delays and resistance-induced relapse represent current challenges plaguing SHH inhibitor therapies. Given that 75% of MBs belong to non-SHH subgroups, it is crucial to identify additional actionable molecular targets. Furthermore, many MB recurrences are metastatic, and MB metastases are clinically and genetically distinct from their matched primary tumor, hence will likely require metastasis specific therapies[12]. It is therefore important to explore the contribution of additional molecular targets such as ion channels towards MB tumorigenesis and metastasis, to facilitate novel therapeutic development.

Ion channels are pore-forming transmembrane proteins that regulate biological processes by controlling ion flow across the membrane. Activation of voltage-gated potassium channels, such as EAG2 (Ether-a-go-go 2), allows potassium ions to flow out of the cell. Emerging evidence has implicated altered ion channel activity in cancer, and revealed that ion channel blockers inhibit cancer cell growth *in vitro*[13–16]. However, few studies have tested ion channel functions during tumorigenesis in animal models, and the potential therapeutic benefit of targeting ion channels *in vivo* to treat CNS cancers, such as MB, remains largely unexplored[17]. Our studies aim to address these important questions.

Herein, we report that *Drosophila* Eag, the founding member of the mammalian potassium channel subfamily that includes EAG2, promotes tumor growth and metastasis in multiple fly brain tumor models. Our cross-species transcriptomic studies delineate common pathways regulated by the EAG2/Eag potassium channels, and reveal that EAG2 and its downstream KCNT2 potassium channel corporate in the regulation of MB cell proliferation. We find that EAG2 channel is enriched at the trailing edge of migrating MB cells to regulate local cell volume dynamics thereby facilitating cell motility, and EAG2 knockdown impairs MB metastasis in a xenograft model. We demonstrate that pharmacological inhibition of EAG2 reduces MB cell viability and motility, and identify an FDA-approved antipsychotic drug, thioridazine, as a novel EAG2 channel blocker with potent efficacy in reducing intracranial xenograft MB growth and metastasis. We show that EAG2 is upregulated in a subset of MB metastases compared to the matched primary tumors from the same patients. Lastly, we present a case report of repurposing thioridazine to treat a human patient with metastasized SHH-MB.

RESULTS

Drosophila Eag promotes brain tumor growth and metastasis

Drosophila emerges as a key model to study brain tumors[18]. For example, overexpression of the bHLH transcriptional repressor Dpn in the neuroblast lineage results in brain tumor formation due to over-proliferation of both type I and type II neuroblasts[19]. Reduced expression of the NHL domain protein Brain tumor (Brat) leads to over-growth of type II neuroblasts[20], while loss of the MBT domain-containing polycomb protein L(3)mbt (Lethal(3) Malignant Brain Tumor) induces over-proliferation of neuroepithelial cells in the optic lobes[21]. Intriguingly, L3MBTL3, the human ortholog of L(3)mbt in fly, is lost in a subset of human MBs with chromosome 6 deletions, and re-expression of L3MBTL3 is sufficient to suppress MB cell growth[22]. Notwithstanding extensive cancer research in *Drosophila*[23], ion channel involvement in cancer has not been reported thus far. Having found EAG2 regulation of MB tumor growth[24], we tested for evolutionarily conserved functions of this potassium channel in cancer, by generating three different *Drosophila* brain tumor models with or without deficiency in *ether-a-go-go* (*eag*) that encodes the fly ortholog of EAG2. Brain tumors were induced by either overexpression of *dpn* (*dpn^{O/E}*) or reduction of *brat* via RNAi knockdown (*brat^{RNAi}*) in the neuroblast lineage driven by insc-Gal4, or loss-of-function mutation of l(3)mbt (Fig. 1a–d). In contrast to the normal appearance of type I and type II neuroblasts in *eag* mutant 3rd instar larvae (Fig. 1e), *eag* loss-of-function mutation (*eag^1*) or expression of dominant negative *eag* (*eag^{DN}*) drastically reduced brain tumor growth (Fig. 1a–b and Supplementary Fig. 1a). Whereas the massive tumor growth caused by *dpn* overexpression led to no survival of 3rd instar larvae raised at 29°C or adult flies raised at 25°C (Fig. 1c), *eag* deficiency reduced tumor size (Fig. 1b and 1d) and enhanced survival (Fig. 1c).

To test whether *Drosophila* Eag potassium channel is involved in tumor metastasis, we adopted a standard allograft assay[25] by transplanting GFP-labeled *dpn*-overexpressing brain lobe tumor cells into the abdominal cavity of wild type host flies (Supplementary Fig. 1b). The open circulation system in fly provides a model for MB metastasis, since MB tumor

cells display limited intraparenchymal invasion but disseminate through mammalian CNS via the circulatory cerebrospinal fluid system. Not only did the transplanted GFP[+] brain tumor cells proliferate to fill up the abdominal cavity in 7–10 days, they also generated metastatic foci in the host brains (Fig. 1f). Mutation of Eag but not Shaker (Sh) potassium channel of the transplanted *dpn*-overexpressing brain tumors markedly reduced tumor growth and metastasis, and extended the survival of host flies (Fig. 1f). Therefore, genetic suppression of Eag channel function limits tumor growth in multiple *Drosophila* brain tumor models and reduces metastasis in a transplantation model.

KCNT2 potassium channel involvement in MB tumorigenesis

To uncover conserved pathways downstream of human EAG2 and fly Eag potassium channels, we performed transcriptomic profiling of human MB cells with or without EAG2 knockdown and *dpn*-driven fly brain tumors with or without *eag* loss-of-function mutation, and carried out pathway enrichment analysis of significance-ranked gene lists[26], as shown in the Enrichment Map[27]. In congruence with the effect of EAG2 knockdown on kinase signaling, mitotic cell cycle and apoptosis[24], human MB cells with EAG2 knockdown and fly brain tumors with *eag* mutation displayed alterations at the transcript level in these pathways as well as those involved in nervous system development, protein catabolism, protein glycosylation, and transmembrane ion transport (Fig. 2a).

We hypothesize that an ion channel network, rather than a single ion channel such as EAG2, intricately regulates cell cycle progression via controlling cell volume dynamics. The cross-species transcriptomic analysis provides an opportunity to identify the candidate ion channel that cooperates with EAG2 during brain tumorigenesis, we therefore focused our follow-up functional studies on the single mammalian ion channel candidate among the 120 orthologous gene pairs displaying similar regulation by EAG2 knockdown in human MBs and *eag* mutation in fly *dpn^{O/E}* brain tumors (Fig. 2a), namely the *KCNT2* gene encoding a potassium channel activated by intracellular sodium and chloride[28]. The KCNT2 potassium channel regulates slow afterhyperpolarization that follows bursts of action potentials, and protects against calcium-induced excitotoxicity during high frequency neuronal firing[29]. *KCNT2* expression was higher in human fetal cerebella compared to adult cerebella (Fig. 2b), and *Kcnt2* was likewise expressed at higher levels in developing mouse cerebella (Fig. 2c). Cerebellar granule neuron precursors (CGNPs) displayed enriched *Kcnt2* expression compared to the cerebellar neural stem cells (NSCs) isolated from pups at postnatal day 7 (P7), whereas treating CGNPs with the Sonic hedgehog (Shh) pathway agonist SAG increased *Gli1* expression without affecting *Kcnt2* (Fig. 2d). *KCNT2* was upregulated in human SHH-MB compared to other MB subgroups (Fig. 2b), and the mouse Shh-MB tumors also displayed upregulation of *Kcnt2* (Fig. 2c), consistent with its high expression in CGNPs. Moreover, *KCNT2* is amplified in a variety of human cancers (Supplementary Fig. 2a), raising the prospect of KCNT2 involvement in multiple cancers. To assess KCNT2 contribution to tumorigenesis, we treated MB cells with short hairpin RNA (shRNA) for KCNT2 knockdown (Supplementary Fig. 2b, c) or with riluzole, a blocker for the persistent sodium current that could activate KCNT2 channels[30]. Both treatments reduced MB cell growth *in vitro* (Fig. 2e). KCNT2 knockdown also slowed tumor growth *in vivo*, and prolonged survival of mice with xenograft of human Vandy-MB-11 of the SHH subgroup

(Fig. 2f). These results demonstrate the functional involvement of KCNT2 during SHH-MB tumorigenesis.

KCNT2 cooperates with EAG2 to regulate mitotic cell volume

To determine its mechanism of action, we next studied KCNT2 subcellular localization during mitosis. KCNT2 resided predominantly at intracellular compartments during interphase, but was enriched to the plasma membrane from metaphase through telophase (Fig. 3a). Temporally, this KCNT2 enrichment to the plasma membrane overlaps with the EAG2 enrichment to the plasma membrane from late G2 to telophase[24]. However, these two potassium channels exhibited largely non-overlapping localization within these human MB cells (Fig. 3a). Remarkably, both potassium channels participate in mitotic cell volume regulation important for MB cell proliferation. Whereas EAG2-deficient MB cells displayed volume increase at the interphase and late G2 phase (Fig. 3b) leading to G2 arrest[24], KCNT2-deficient MB cells exhibited cell volume increase at the prometaphase and metaphase associated with prolonged mitosis and mitotic catastrophe (Fig. 3b–c). We also tested whether overexpressing KCNT2 would impact COS7 cell volume and morphology. Overexpression of both EAG2 and KCNT2 decreased the cell volume to a greater extent than overexpression of EAG2, whereas overexpression of KCNT2 appeared to change COS7 cell morphology without reducing the overall cell volume (Fig. 3d), indicating that KCNT2 cooperates with EAG2 to regulate the cell volume. Thus, our cross-species studies identified a novel potassium channel with a critical role in regulating MB tumorigenesis, and revealed a co-option mechanism for different potassium channels to control cell volume dynamics critical for mitotic success and tumor growth (Supplementary Fig. 3).

EAG2 involvement in MB metastasis and MB cell migration

Next we asked whether EAG2, like Eag in *Drosophila* (Fig. 1f), is important for metastasis of human MB cells implanted in mice, by performing longitudinal non-invasive bioluminescence imaging of MB tumors with or without EAG2 knockdown. Whereas a majority of mice bearing control MB tumors developed intracranial (56%; 5/9) and spinal cord (67%; 6/9) metastases within several weeks, mice bearing MB tumors with EAG2 knockdown displayed no metastasis even after acquiring greater tumor burden at the engraftment sites months later (Fig. 4a). Histopathological analyses confirmed the confinement of xenografted tumors with EAG2 knockdown to the injection sites, whereas control tumors extensively disseminated to the leptomeningeal spaces (Fig. 4b). These results demonstrate that EAG2 promotes MB metastasis, a function distinct from its role in driving primary tumor growth.

Leptomeningeal metastasis is a cardinal feature of malignant MB with greater recurrence risk. The standard treatment of metastases with craniospinal radiation is associated with high morbidity, secondary malignancies, and severe impact on intelligence[31]. It is therefore important to pursue *in vitro* and *in vivo* studies for development of novel therapies. Critical for malignant dissemination, cell motility requires polarized morphology with lamellipodia at the leading edge and contracting cell rear at the trailing edge. Formation of these dynamic structures involves local volume changes. While localized potassium channel activity at the trailing edge has been hypothesized to drive cell rear contraction, it is unknown whether any

potassium channel is specifically localized to the trailing edge[17]. Remarkably, whereas EAG2 displayed an intracellular distribution distant from the plasma membrane in non-migrating MB cells, it enriched at the cell rear and localized to the trailing edge during spontaneous and directed migration (Fig. 4c and Supplementary Fig. 4). Moreover, EAG2 knockdown markedly reduced the motility of MB cells without affecting directionality, as did the EAG2 channel blocker astemizole, a known EAG2 channel blocker with an IC_{50} of ~1.5 μM[32] (Fig. 4d–f). While control cells exhibited polarized morphology with lamellipodia at the fan-shaped leading edge and contracting trailing edge, EAG2-deficient MB cells failed to polarize or contract the cell rear (Fig. 4g–i). By contrast, KCNT2 did not enrich to the trailing edge of MB cells (Supplementary Fig. 5a) nor did it modulate their migratory morphology (Supplementary Fig. 5b–d). These findings indicate that, while KCNT2 and EAG2 cooperate to regulate MB cell mitosis, EAG2 functions as the primary potassium channel for the local outflow of potassium ions at the trailing edge important for MB cell motility. Therefore, the beneficial effect of EAG2 knockdown or channel block is likely through a combination of two aspects: impairing MB cell mitosis by reducing the activity of EAG2 and KCNT2, and reducing MB cell motility by decreasing cell rear retraction.

Thioridazine blocks EAG2 and reduces MB tumorigenicity

To identify novel EAG2-blocking agents as potential MB therapeutics, we screened a series of HERG channel-blocking, FDA-approved antipsychotics for their efficacy in inhibiting MB cell growth. Based on the structural similarity of EAG2 and HERG, this strategy facilitates the identification of candidate drugs, which require precautions routinely exercised by physicians to guard against potential risk of arrhythmia. We found that the *in vitro* growth of Vandy-MB-11, *Math1-Cre; SmoM2* and *Ptch1^{+/−}; p53^{−/−}* cells was reduced by thioridazine (Mellaril), and to a lesser extent by promazine, at low μM concentrations close to the IC_{50} for EAG2 channel block (Fig. 5a–d **and** Supplementary Fig. 6), as did EAG2 knockdown[24]. In contrast, D283 and GTML cells, which displayed lower EAG2 expression[24], were only affected by thioridazine at higher concentrations (Fig. 5d). Importantly, treating MB cells with E-4031, a selective HERG channel blocker with nM IC_{50} that does not block EAG channel[33], had little effect on MB cell growth (Fig. 5d). Global application of thioridazine impaired human MB cell rear retraction, migratory polarization, and motility (Fig. 5e–g), recapitulating the phenotype of EAG2 knockdown and astemizole treatment (Fig. 4f–i). Furthermore, local application of the EAG2 channel blocker thioridazine to the cell rear reduced the rear retraction velocity (Fig. 5h), supporting the model that enriched EAG2 potassium channel activity at the trailing edge regulates local volume reduction to promote cell rear contraction and cell motility (Supplementary Fig. 7). As phenothiazines with a tricyclic ring, thioridazine and promazine are structurally distinct from astemizole (Fig. 4e and 5a, and Supplementary Fig. 6a). The similar effects of thioridazine, astemizole and EAG2 knockdown (Fig. 4f–i and 5d–g, and Supplementary Fig. 8a) thus indicate that thioridazine reduces MB cell growth and motility by blocking EAG2 channels. Moreover, thioridazine treatment of MB cells for three days reduced *KCNT2* expression (Supplementary Fig. 5e), similar to the effect of EAG2 knockdown (Fig. 2a). It thus appears that thioridazine block of EAG2 potassium channel not only compromises its volume regulation crucial for human MB cell proliferation and motility, but also reduces the

activity of KCNT2 potassium channel as a downstream effector of EAG2 channel activity (Supplementary Fig. 3).

Thioridazine reduces xenograft MB growth and metastasis

As an antipsychotic for treating schizophrenia – a drug that has been in use for over 40 years, thioridazine readily crosses the blood-brain barrier (BBB)[34]; repetitive dosing allows µM plasma concentration to be achieved with widespread brain distribution in human patients[35][36]. Therefore we tested the efficacy of intraperitoneal injections of thioridazine in treating xenograft MB tumors in mice. We began the treatment at day 26 post implantation of human MB tumor cells that express EAG2 either at high level (Vandy-MB-11) or at low level (D283) (Fig. 6a–c) into mice, when the bioluminescence imaging already demonstrated prominent tumor burden (Fig. 6d). As expected for an EAG2 channel blocker, thioridazine (daily injection at 25 mg/kg for 2 weeks) did not affect the xenografted D283 tumors, but caused substantial tumor regression, reduced intracranial metastasis, and prevented spinal cord metastasis in mice bearing human Vandy-MB-11 tumors with high EAG2 expression, thereby prolonging their survival (Fig. 6a and 6c). Of the eighteen mice subjected to thioridazine treatment at 25 mg/kg, two mice exhibited complete and sustained regression of both primary and metastasized Vandy-MB-11 MB tumors (Fig. 6d). Thioridazine treatment at lower dosages (5 mg/kg or 15 mg/kg) provided less therapeutic benefit, but resulted in sustained tumor regression in one mouse in the 15 mg/kg treatment group (Fig. 6c). Notwithstanding its inability to cross the BBB, astemizole treatment for 2 weeks reduced subcutaneous allograft of mouse MB *in vivo* (Supplementary Fig. 8b–d). The ability of two structurally unrelated EAG2 channel blockers to reduce MB growth *in vivo* in mouse models, taken together with the specific effects of thioridazine in curbing the growth and metastasis of xenograft human MB with high but not low EAG2 expression, point to EAG2 as a promising target for treatment of MB that displays high EAG2 expression.

EAG2 upregulation in metastatic MB of subsets of patients

In support of the EAG2 involvement in promoting MB metastasis in human patients, quantitative PCR of both primary tumors and metastatic nodules (met-MBs) of molecularly subgrouped MBs from the same patients revealed that 80% (8/10) of the met-MBs displayed >1.5 fold *EAG2* upregulation compared to matched primary MBs in group 3 patients (Fig. 7a), and 18% (2/11) of the met-MBs showed >1.5 fold *EAG2* upregulation compared to matched primary MBs in group 4 patients (Fig. 7b). Since the available matched primary and metastatic human MB samples did not include SHH-MBs, we examined the *Ptch*^{+/−}/ *Math1-SB11/T2Onc2* Sleeping Beauty mouse model[12] in immunohistochemical analyses, and found 37.5% (6/16) of metastasized Shh-MB tumors displaying higher Eag2 expression than primary tumors in the same mice (Fig. 7c). The finding of elevated EAG2 expression in metastatic lesions raised the prospect that EAG2 may promote MB metastasis or tumor growth at the disseminated site.

Case report for thioridazine treatment of a MB patient

Our studies suggest that EAG2 channel blockers that can penetrate BBB, such as thioridazine, may display therapeutic efficacy to treat human MB with high EAG2

expression. For this reason, we identified a 22 year-old male patient with metastatic SHH-MB and robust EAG2 expression at his iliac lesion (Fig. 8a). This patient was initially diagnosed in 2009 with localized MB of the posterior fossa, and underwent a gross total resection followed by craniospinal irradiation therapy in combination with temozolomide. In 2011 the patient was diagnosed with relapse metastatic MB after complaining of localized knee pain, and underwent high dose chemotherapy with cisplatin, cyclophosphamide and vincristine followed by four autologous stem cell transplants. That regimen was followed with 6 cycles of cis-retinoic acid and vorinostat. In 2012 the patient had further evidence of widespread metastasis with immunohistochemical evidence of SHH activation, and started on palliative chemotherapy with cycles of metronomic chemotherapy including celebrex, vismodegib (a SHH signaling inhibitor that targets the SMO receptor) and alternating etoposide and temozolomide. Imaging demonstrated disease progression after 7.5 months of this palliative metronomic chemotherapy. At that time the patient transferred care to our institution for consideration of an alternative therapy regimen. His iliac tumor was tested positive for EAG2 (Fig. 8a), so thioridazine was added to the same palliative metronomic chemotherapy regimen administered thus far. The patient received thioridazine in dose escalation for approximately two months, starting with 50 mg thioridazine twice daily until the dose was raised to 150 mg in the morning and 175 mg in the evening, while his other chemotherapy regimen was held constant. During initial consultation and throughout treatment, his primary brain tumor site remained in remission. Baseline transaxial fused PET/CT images of the pelvis before thioridazine treatment identified a large hypermetabolic right iliac mass. Comparison with images of this region taken after the two-month thioridazine treatment revealed a reduction of the lesion from 9.4×5.4 cm to 8×4 cm in size, and from SUVmax 13.5 to SUVmax 8.2 in FDG avidity, suggestive of a metabolic response to the thioridazine therapy since all other anti-tumor medications remained unchanged throughout (Fig. 8b). Given known risks of HERG channel blockers in arrhythmias, tardive dyskinesia, akathisia, hepatotoxicity and leukopenia, the patient was monitored with biweekly metabolic panels, comprehensive blood counts and EKGs in tandem with clinical visits and exams. The patient did not have adverse effects of QT prolongation or any of the above listed toxicities. However, the patient did not tolerate prolonged medication due to marked emotional lability and depression. Ultimately, despite trials of other chemotherapeutic regimens and radiation, the patient died of progressive disease nine months after cessation of thioridazine treatment. The results seen in our patient are encouraging for targeting EAG2 channel as a potential therapy in MB. However, we emphasize caution given the singular case described here and considerable potential side effects that could impact tolerance of thioridazine.

DISCUSSION

MB is the most common malignant pediatric brain tumor, and a major cause of pediatric morbidity and mortality. Standard care with surgery, radiation and chemotherapy commonly results in serious cognitive and neuroendocrine deficits that can substantially impact the quality of life. Secondary malignancies due to metastasis or radiotherapy further compromise the prognosis. While the five-year survival rate for average-risk MB patients is 60–70%, the survival rate of high-risk MB patients with metastasis is 20–40%[31]. These

clinical considerations underscore the urgency to identify novel molecular targets and develop targeted therapies that may one day replace the non-selective chemotherapy and radiotherapy with debilitating side effects, and to effectively combat metastasis. To this end, we have focused on studying ion channels, prompted by our recent finding of EAG2 function in MB cell cycle progression[24]. Using multiple *Drosophila* brain tumor models induced by oncogene overexpression or loss of tumor suppressors to complement our study of mice with xenografted human MB cells, we show that the functions of EAG2/Eag channel to promote malignant growth and metastasis are evolutionarily conserved (Fig. 1). Our cross-species studies identify common pathways and genes, including the SHH-MB-enriched potassium channel KCNT2, regulated by the mammalian EAG2 channel and fly Eag channel during tumorigenesis (Fig. 2). Having found that KCNT2 localizes to the plasma membrane starting at metaphase, we report that KCNT2 and EAG2 potassium channels coordinate to regulate mitotic volume, MB cell proliferation, and MB tumor growth (Fig. 3). EAG2 localizes to the trailing membrane of migrating cells where it promotes local cell volume reduction, and enhances cell motility and tumor metastatic potential (Fig. 4). We provide evidence that the known EAG2 channel blocker astemizole reduces MB cell migratory polarization and cell rear contraction, and impairs MB cell viability, motility and allografted tumor growth (Fig. 4 and Supplementary Fig. 8). We identify the FDA-approved antipsychotic drug thioridazine as a novel EAG2 channel blocker (Fig. 5), which demonstrates efficacy in reducing MB growth and metastasis within the central nervous system (Fig. 5 and Fig. 6). We show that EAG2 is upregulated in a subset of MB metastases compared to their matched primary tumors (Fig. 7). We further present a case report as to how repurposing this drug for treating a human patient with metastatic SHH-MB was associated with clinical response (Fig. 8).

Evolutionarily conserved EAG2/Eag function in brain tumors

By generating multiple *Drosophila* brain tumor models, we found that Eag channel deficiency reduces brain tumor growth and metastasis. Our bioinformatics analyses establish a roadmap to elucidate the conserved pathways that EAG2/Eag potassium channels regulate for brain tumorigenesis. With the streamlined genome complexity in *Drosophila* and the ability to conduct large-scale genetic and *in vivo* chemical screens for anti-cancer agents[37], our findings not only provide the first example for an ion channel involvement in malignant tumor growth in *Drosophila,* but also stimulate investigation of ion channel functions in tumorigenesis capitalizing the powerful fly genetics.

Coordinated potassium channel regulation of tumor growth

Pronounced cell shape and volume changes accompany cell cycle progression. The proliferating cells increase volume at interphase, rapidly condense cytoplasmic volume prior to mitotic entry through a process known as pre-mitotic cytoplasmic condensation (PMC), reach a minimal volume at metaphase and achieve mitotic rounding, followed by volume increase and cytokinesis to generate two daughter cells[38, 39]. Having previously shown that EAG2 enriches to the plasma membrane at late G2 and M phase[24], we found KCNT2 to be another potassium channel displaying cell cycle phase-specific plasma membrane localization critical for mitotic volume regulation (Fig. 2 and Fig. 3). As KCNT2 is

frequently amplified in multiple human cancers (Supplementary Fig. 2a), the identification of specific KCNT2 channel blocker may be of high therapeutic interest.

EAG2 potassium channels for MB metastasis

Cell motility critically depends on local volume regulation. The cell volume first increases at the leading edge with lamellipodia protrusion and then decreases at the rear end for its retraction[40–42]. In the case of MDCK-F cells, application of the IK1 Ca^{2+}-activated K^+ channel blocker charybdotoxin to the trailing edge inhibits migration[43] and increases cell volume[44]. However, IK1 channels are more concentrated at the cell front[45], indicating IK1 channels at the rear end may be preferentially activated owing to dynamic Ca^{2+} oscillations in migrating cells[40, 41]. Our studies have revealed a direct mechanism employed by migrating MB cells: upregulation (Fig. 7) and translocation of EAG2 channels to the trailing edge to facilitate MB cell migration and metastasis (Fig. 4). It is important to note that impaired cell motility might not be the sole cause underlying the metastasis defect associated with EAG2 knockdown (Fig. 4).

Therapeutic potential of EAG2 blockers for MB treatment

Ion channels are highly druggable targets, owing in large part to their membrane localization. Our findings that EAG2 channel regulates both primary MB tumor growth and metastasis provides strong impetus for considering EAG2 channel blockers as MB therapeutics. In this study, we demonstrate the proof of principle use for ion channel blockers in treating brain tumor. EAG2 channel blockers with inhibitory actions on the closely related HERG channel, which regulates the repolarization phase of the cardiac action potential, may induce cardiac arrhythmia. Therefore close monitoring of the possible side effects, as has been clinically practiced for patients regularly receiving thioridazine treatment, is important. Our discovery encourages the future development of second-generation drugs with greater specificity for blocking EAG2 channels as well as substantial CNS access and better toxicity profile.

ONLINE METHODS

Bioinformatics studies

Gene expression analysis—Total RNA from Vandy-MB-11 cells was extracted. DNAse was used to remove genomic DNA. The RNAs then were assessed by electrophoresis and Agilent 2100 Bioanalyzer to ensure quality before subjecting to gene expression array using Affymetrix Human Gene 2.0 ST. For fly microarray, 20–50 brains from control, $dpn^{O/E}$ or $dpn^{O/E}$; eag^1 3rd instar larvae were dissected, pooled and dissociated using trypsin. GFP+ neuroblast lineage cells in the brain tumors were FACS-sorted. Total RNA was extracted from 20,000–40,000 neuroblasts using Ambion RNAqueous-Micro kit. For each sample, 100 ng mRNA was amplified, labeled and hybridized to SurePrint G3 Custom Array representing custom-designed 60,000 *Drosophila* transcripts and manufactured by Agilent Technologies. Gene expression values were pre-processed separately for human and fly microarrays using the quantile rank normalization method from the aroma.light R package. Differential gene expression values were computed with linear regression methods of the Limma R package. Statistical significance of

differential expression was computed with the empirical Bayes moderated t-test to account for small sample sizes. P-values were corrected for multiple testing with the Benjamini-Hochberg False Discovery Rate (FDR), and only genes with statistically significant alterations were retained for pathway enrichment analysis (FDR p<0.05).

Pathway enrichment analysis—Analysis of enriched functions and pathways was carried out independently for genes in human and fly. To emphasize genes with the strongest transcriptional change, genes were ranked according to statistical significance (FDR p-value) and analyzed with the ordered gene list enrichment method in the g:Profiler software[26]. To only account for information natively curated for human and fly, we performed functional analysis of biological processes of Gene Ontology (GO) and discarded other sources of functional evidence. GO gene sets with more than 500 genes in total, and sets with less than three differentially expressed genes were filtered. GO gene sets that were only present in the fly ontology were also left out. Results were corrected for multiple testing with default g:Profiler methods and filtered for significance (corrected p<0.05). Two-color network visualization of enriched pathways in human (nodes with red cores) and fly (nodes with blue edges) was constructed with the Enrichment Map plugin of Cytoscape. Enriched functions, and pathways were connected by edges if their gene sets overlapped by more than 60% according to the Jaccard+overlap measure. Finally, network-clustered groups of pathways were manually curated for common functional themes and filtered for themes conserved in human and fly.

RNA extraction, reverse transcription and real-time RT-PCR

For human tumors, RNA was isolated and purified using Trizol reagent (Life Technologies). 1 μg of RNA was reverse transcribed to cDNA using Superscript III First-Strand Synthesis SuperMix for qRT-PCR (Life Technologies). Quantitative PCR was prepared with TaqMan Universal Master Mix II, with UNG (Applied Biosystems) *Eag2* probe Hs00544949_m1 and Human *GAPD* (*GAPDH*) Endogenous Control 4310884E. Tumor cDNA (75 ng/well) was prepared in triplicate and analyzed using a Step One Plus Real-Time PCR System (Applied Biosystems). Each tumor/metastasis pair was analyzed using the Ct method and normalized to the primary tumor sample. Standard error of the mean was used to calculate error.

For mouse tumors and human MB cells, total RNAs were extracted using RNAeasy Mini kit (Qiagen) and treated with DNAse to remove genomic DNA. 2 μg of RNA was reverse transcribed to cDNA using iScript cDNA Synthesis Kit (Bio-Rad). All DNA and RNA concentrations were measured by NanoDrop 1000 Spectrophotometer. Real-time detection and quantification of cDNAs were performed with the iCycler instrument (Bio-Rad). qPCR was performed in a 20 μl reaction mixture using SYBR@GreenER qPCR Supermixes (Invitrogen). 50 cycles of amplification was performed according to manufacturer's instructions. Fluorescence data were collected at annealing stages and real-time analysis performed with iCycler™ iQ Optical System Software V3.0a. Serial dilutions of cDNAs were used for construction of the standard curve. Ct values were determined with automatically set baseline and manually adjusted fluorescence threshold. Gene expressions were normalized with that of *Gapdh* and analyzed using the Ct method. All experiments

were repeated three times. The mouse *Kcnt2* qPCR primers are: forward, TCCGCTTGTTCAACTTTTCC; reverse, AAACCCCATAAAGGTAGACTTCG. The human *KCNT2* qPCR primers are: forward, GGATACGCCTGTTCAATTTTTC; reverse, TGTAAGCCCCACAAAGGTAGA.

Immunohistochemistry and quantification of Eag2 staining

All immunohistochemistry analyses were performed on tissue sections collected from OCT- or paraffin-embedded tissues. The primary antibodies were rabbit anti-Eag2 (Abcam, 1:200), rabbit anti-phospho-Histone 3 (Millipore, 1:400). Apoptosis was detected using the ApopTag® Fluorescein In Situ Apoptosis Detection Kit (Millipore). For the quantification of Eag2 staining signal in the $Ptch^{+/-}/Math1\text{-}SB11/T2Onc2$ tumors, we imaged stained tissues at five randomly selected fields at 200x magnification for each matched primary or metastasized tumor, and utilized the following scoring criteria: if 0% of the total cells is positive in a filed: the score is 0; 1–10% positive: 1; 11–20% positive: 2; 21–30% positive: 3; 31–40% positive: 4; 41–50% positive: 5; 51–60% positive: 6; 61–70% positive: 7; 71–80% positive: 8; 81–90% positive: 9; 91–100% positive: 10. The data is expressed as mean ± SEM. The average score of each primary tumor was compared with the average score of the matched metastasized tumor. Statistical analysis was performed using paired Student's t-test. Note that Eag2 antibody was used at high dilution (1:2000) to reveal the expression level difference for statistical analysis, while the dilution of 1:200 was used to demonstrate that primary tumors express Eag2 albeit at lower levels as shown in the left panels of Fig. 7c.

Lentivirus-mediated shRNA analyses

Human pLKO.1 lentiviral shRNA target gene set against *EAG2*, *KCNT2* and pLKO.1-TRC-control vector were obtained from Open Biosystems. The concentrated lentiviral particles were generated by the UCSF Viracore. Virus infections were performed within antibiotics-free culture medium for 24 hours. Final concentration of 10 μg/ml polybrene (Millipore) was added into the culture medium to enhance virus infection efficiency. The specific sequence of the *EAG2* shRNAs is previously reported[24]. *KCNT2* shRNA mature antisense sequences are: #1: ATCACCACATAATAATCCTGG; #2: ATAGGTCTTGATCTTTAAGGG; #3: ATAAGGTGGGTAACCTTTAGC.

Culture of MB cells and cerebellar neural precursor cells

Primary human Vandy-MB cells were derived from the resected tumors from patients admitted to Vanderbilt University Medical Center (VUMC). MB specimens from patients treated at the VUMC were obtained in accordance with the Institutional Review Board's approval. Tumor samples were dissociated with Papain (Worthington Biochemical Corporation) and plated in DMEM/F12, 10% FBS, and 1X penicillin–streptomycin. Cells from three patients, Vandy-MB-6, Vandy-MB-10 and Vandy-MB-11 were successfully maintained with DMEM with 10% FBS and propagated using standard tissue culture protocols. Vandy-MB-11 cells were derived from a biopsy of an 11-year old male patient who developed medulloblastoma with extensive nodularity (MBEN) at the cerebellar vermis location. The SF8953-MB cells were derived from resected tumor of a 7-years old female

patient who developed anaplastic MB and was admitted to the UCSF Medical Center. The SF8953-MB cells were maintained with DMEM with 10% FBS and propagated using standard tissue culture protocols. The immunofluorescence-staining experiments were conducted using cells under 5 times of passages. The DAOY MB cell lines were obtained from ATCC and maintained using DMEM with 10% FBS. Primary mouse MB cells were established from freshly dissected tumors developed in *Math1-Cre; SmoM2* mice according to previously reported protocols[46][47]. The mouse MB cells were cultured with neural basal medium supplemented with glutamine, N2, B27, 25 ng/ml basic FGF and 25 ng/ml human EGF without addition of serum. $Ptch1^{+/-}; p53^{-/-}$ cells were established from MBs developed in $Ptch1^{+/-}; p53^{-/-}$ mice and maintained with DMEM with 10% FBS as previously described[48]. Isolation and primary culture of cerebellar neural stem cells and cerebellar granule neuron precursor cells from P7 postnatal pups were performed as previously described[49][50]. 200 nM of SAG was added to the cerebellar granule neuron precursor culture medium to stimulate Shh pathway activation. All cell lines were regularly checked for mycoplasma infections and treated with Plasmocin (Invivogen) when infection was noted. No cell lines are listed in the database of commonly misidentified cell lines maintained by ICLAC and NCBI Biosample.

Immunofluorescence staining was performed using 4% PFA fixed cells with standard protocol. The primary antibodies used were rabbit anti-EAG2 (Alomone Labs, 1:4000), rabbit anti-EAG2 (LSBio, 1:1000), rabbit anti-EAG2 (Abcam, 1:1000), rabbit anti-phospho-Histone 3 (Millipore, 1:2000), rabbit anti-GM130, clone EP892Y (Abcam, 1:1000) and mouse anti-KCNT2 (NeuroMab, 1:50). F-actin was labeled with Alexa Fluor 633 Phalloidin (Molecular Probes, 1:200). To determine the clonogenic potential of MB cells, cells were plated at clonal density (150 cells/ml of culture medium) into 60 mm plates with indicated concentrations of astemizole or vehicle. Cell colonies were stained with 0.05% crystal violet 7–10 days after seeding. Representative results from three independent experiments were shown for all clonogenic assays. Normalized incidence of mitotic catastrophe was defined as percentage of cells with mitotic catastrophe within all the cells that entered mitosis. For the cell viability assay, 500 MB cells were seeded into one well of the 96-well plate, drugs were added 3 hours after seeding and the cells were incubated for 3 days, followed by the cell viability assay using the CellTiter 96® AQueous One solution.

Immunoblotting

For Western analysis, total proteins were extracted using a lysis buffer containing 50 mM Hepes (pH 7.4), 150 mM NaCl, 1% NP-40, 1 mM dithiothreitol (DTT), 1 mM EDTA supplemented with Complete Protease Inhibitor Cocktail (Roche). Protein lysate samples, 100 μg each, were resolved on 4–12% Bis-Tris gels using MOPS buffer (Invitrogen) and transferred onto a PVDF (Millipore) membrane using a buffer containing 25 mM Tris base, pH 8.3, 192 mM glycine, and 20% methanol for 1 hour at 100 V at 4°C. Western blot assays were performed using primary antibody diluted in TBS supplemented with 0.1% Tween-20 and 0.65% milk. Immunoreactive bands were visualized using horseradish peroxidase-conjugated secondary antibodies (Amersham), followed by chemiluminescence with ECL-plus Western Blotting Detection System (Amersham). Chemiluminescence was imaged and analyzed using Molecular Imager@VersaDoc MP4000 system (Bio-Rad). The primary

antibodies used were: rabbit anti-EAG2 (Alomone, 1:1000), and mouse anti-αTubulin (Sigma, 1:10000).

3-D reconstruction of cells

In order to visualize cell morphology and determine cell volume, we expressed soluble GFP in MB cells and performed serial imaging using our Leica TCS SP5 confocal setup. We acquired the image stacks with a Z step size at 0.17 μm per optical slice using a 63X 1.4 NA oil lens throughout the entire thickness of the cells. The confocal LIF files were converted into Imaris file through ImarisFileConverter 6.4.2. All subsequent image processing was conducted with Imaris 5.5 software. A region of interest encompassing a single cell or a local cellular region was chosen for 3-D reconstruction. A smooth level of 0.2 was given to every measurement for consistency.

Since EAG2 channel localizes to the plasma membrane, its capacity to permeate ion directly regulates cytoplasmic volume by controlling cytoplasmic osmolarity. We consider measuring the cytoplasmic volume a direct readout for its regulation of volume changes. In order to calibrate our method for volume measurement, we performed volume measurement of fluorescent spherical beads of 4 and 6 μm in diameter using the same imaging method we used for our cell studies. Our calculated volume (mean ± SEM) for the 4 μm-diameter beads is 33. 61 ± 0.43 μm^3 with 95% Cl at $32.70 - 34.52$ μm^3, and for the 6 μm-diameter beads is 112.3 ± 1.81 μm^3 with 95% Cl at $108.5 - 116.1$ μm^3. The expected volume for the spherical beads of 4 and 6 μm diameters are 33.5 μm^3 and 113.1 μm^3, respectively, which all fall in the 95% CI of our calculated volumes. Since the dimensions of MB cells are larger than 6 μm, these calibrations suggest that our imaging and volume quantification method is of sufficient accuracy for cellular comparisons.

Xenograft, *in vivo* imaging and thioridazine treatment

Tumor cells with firefly-luciferase-expressing reporter—MB cells were transduced with a lentiviral vector containing firefly luciferase (Fluc) under the control of the spleen focus forming virus (SFFV) promoter. Cells were screened for infection efficiency by treatment with luciferin (D-luciferin potassium salt, 150 mg/kg, Gold Biotechnology, St Louis, MO) *in vitro* and examination by a Xenogen IVIS Lumina System (Xenogen Corp., Alameda, CA). More than 95% of cells were infected.

Surgical procedure for implantation of tumor cells—Five weeks-old female *nu/nu BALB/C* immunodeficient mice were purchased from Simonsen Laboratory. Animals were housed under aseptic conditions, which included filtered air and sterilized food, water, bedding, and cages. Tumor cells were implanted into the brains as previously described[24]. Briefly, mice were anesthetized by intraperitoneal injection of a mixture containing 100 mg/kg of ketamine and 10 mg/kg of xylazine in 0.9% saline. The skull of the mouse was exposed and a small opening was made using 25 gauge needle (PrecisionGuide) at 3.0 mm to the right of the midline and just behind the bregma. At this location, 1.0×10^5 Vandy-MB-11 cells in 3 μl Hanks' Balanced Salt Solution without Ca^{2+} and Mg^{2+} (HBSS) was slowly injected (over 1 minute) into the right caudate putamen at 3.0 mm deep from the underside of the skull. All procedures were carried out under sterile conditions.

In vivo bioluminescence monitoring—*In vivo* bioluminescence imaging was performed with the Xenogen IVIS Lumina System coupled LivingImage software for data acquisition (Xenogen Corp.). Mice were anesthetized with 100 mg/kg of ketamine and 10 mg/kg of xylazine and imaged 10 min after intraperitoneal injection of luciferin. Signal intensity was quantified within a region of interest over the head that was defined by the LivingImage software.

Thioridazine treatment—A two-week daily intraperitoneal injection of thioridazine at 5, 15, or 25 mg/kg began at day 26 after tumor cell implantation when significant tumor burdens were detected. Intracranial MB tumor and metastasis were monitored with *in vivo* imaging before, during and after thioridazine treatment. We observed occasional weight loss in thioridazine-treated mice, and stopped the treatment in mice displaying weight loss over 15%. We observed that mice regained weight after treatment cessation.

Subcutaneous allograft and astemizole treatment

Math1-Cre; SmoM2 MB tumors were acutely extracted and minced into small tissue pieces with fine forceps in Accutase solution, followed by incubation at 37°C for 10–20 minutes until the tumor tissues were dissociated into mostly single cells or small cellular aggregates under microscopic inspection. Equal volume of neural stem cell medium (neural basal medium supplemented with glutamine, N2, B27, 25 ng/ml basic FGF and 25 ng/ml human EGF without addition of serum) was added into the Accutase solution followed by spinning at 1000x RPM for 3 minutes. After spinning, the supernatant was removed and the tumor cells were resuspended in neural stem cell medium. Equal volume of pre-cooled Matrigel (BD Biosciences) was added into the medium to achieve a concentration of 5×10^6 cells per 200 μl of injection per mouse. Cell mixture was loaded into pre-cooled syringe without bubble formation. The pre-cooled needle was subcutaneously inserted into the mouse flank. It was important to sway the needle several times after insertion to create the appropriate space for tumor cells to distribute into the pocket. A total of approximately 5×10^6 tumor cells in 200 μl medium were implanted.

Astemizole was purchased from Tocris Bioscience, and dissolved in Ora-Plus oral suspending vehicle (Paddock) with vortex and sonication to achieve stock concentration of 10 mg/ml. Once palpable tumors are detected one week post implantation, daily oral gavage of 50 mg/kg astemizole to the mice was performed for two weeks. Tumor sizes were measured daily with caliber and the tumor volume (mm^3) was calculated as $\frac{1}{2} \times$ length $\times$ width^2 (the length and width are in mm).

Mice

Math1-Cre, *SmoM2* and *Ptch1$^{+/-}$* mice are obtained from the Jackson Laboratory. Five weeks-old female *nu/nu BALB/C* immunodeficient mice were purchased from Simonsen Laboratory. Mice were housed in an animal facility and were maintained in a temperature-controlled and light-controlled environment with an alternating 12-hour light/dark cycle. A maximum of five mice were housed in one cage. All protocols have been approved by the UCSF Institutional Animal Care and Use Committee.

Local superfusion of thioridazine to MB cells

The functional requirement of localized EAG2 channel activity for rear retraction during MB cell migration was studied by local superfusion of thioridazine. Vandy-MB-11 cells were plated on glass coverslips four days before experiments. The cells were maintained in DMEM medium supplemented with 10% FBS and 10 mM HEPE buffers at 37°C during the course of drug application and imaging. Cells with clear migratory polarization (flat and extending lammelipodia, retracting cell rear) were randomly selected for superfusion of vehicle or thioridazine. Cell rear retraction was monitored under phase-contrast microscopy over a total of 12 minutes with 6 minutes intervals. For precise local superfusion, a glass pipette with tip opening diameter of 20–25 µm filled with vehicle (PBS) and thioridazine (10 µM) was brought to the close vicinity of the cell rear using a micromanipulator. Pre-heated vehicle and thioridazine were constantly superfused using the PR-10 pressure regulator (ALA Scientific Instruments,) at 4 kPa. A defined stream of solution was visible and applied over only the rear part of the cell. Cell rear retraction velocity was calculated by the distance of rear displacement over time (µm/minute). Twenty randomly selected cells were studied in both vehicle and thioridazine group. Similar experiments were performed with thioridazine application to the front of migrating cells.

Electrophysiological studies

COS7 cell preparation—COS7 cells were plated on coverslips and transfected with wild type EAG2 channel. Recordings were performed 1–2 days after transfection. Cells were placed in an electrophysiology recording chamber at room temperature and bathed with (in mM) 145 NaCl, 4.8 KCl, 2 $MgCl_2$, 1.1 EGTA, 10 HEPES, pH 7.2 with KOH.

Patch clamp recordings—Whole cell patch clamp recordings were performed at room temperature, with an internal solution consisting of (in mM): 130 K Gluconate, 10 HEPES, 1 EGTA, 2 $MgCl_2$, 0.1 $CaCl_2$, 4 Na_2-ATP, 0.3 GTP, pH7.2 with NaOH. Patch electrodes (borosilicate glass) with a resistance between 3 MΩ and 8 MΩ were used; pipette and whole cell capacitance were compensated. Series resistance was less than 20 MΩ at all times and compensated >80%. Any recording in which series resistance exceeded 20 MΩ or became unstable with compensation was terminated and not used as part of the analysis. Voltage steps were given from −100 mV to +100 mV with 20 mV increments. Outward current amplitude was determined using a leak-subtracted step in voltage clamp by holding potential at +60 mV. I–V curve was generated by plotting current amplitude at different voltages.

Drosophila studies

Fly Stocks—The following fly stocks were used:

Abbreviation	Genotype	Characterization	Reference
$dpn^{O/E}$	+; insc-Gal4; UAS-dpn	Ectopic expressing dpn in neuroblasts (NB) results in NB over-proliferation and brain tumor formation.	19, 51
eag^1	eag^1; +; +	Loss-of-function, expresses eag protein with truncated C-terminus.	52

Abbreviation	Genotype	Characterization	Reference
eag^{DN}	$+; UAS- eag^{932}; +$	Dominant negative, ectopically expresses truncated eag protein with only 192 amino acids of the N-terminal hydrophilic domain.	[53]
$brat^{RNAi}$	$+; insc- Gal4/UAS- brat^{RNAi}; +$	Knockdown brat, a tumor suppressor, in NBs results in over-proliferation of mainly type II NBs and brain tumor formation.	[20]
$l(3)mbt$	$l(3)mbt^{ts1}$	Temperature sensitive loss-of-function allele of tumor suppressor lethal (3) malignant brain tumor, produces inactive l(3)mbt at non-permissive temperature, which results in over-proliferation and brain tumor formation	[21]
Sh^{14}	$Sh^{14}; +; +$	Missense mutation in the core region results in non-functional shaker channel	[54]

For transplantation study, *insc-Gal4; UAS-mCD8-GFP* was introduced into each tested lines to visualize tumor growth. w^- virgin females were used for all controls. Additional information on the function of these alleles and genes can be found in Flybase (http://www.flybase.org).

Fly culture—All larvae and flies were kept at 25°C unless otherwise specified. For the experiments involving *l(3)mbt* tumor model, 29°C was used to inactivate temperature-sensitive l(3)mbt and induce tumor formation. For *insc-Gal4/UAS* driven overexpression system, higher temperature promotes stronger expression of UAS-activated genes thus induces more severe phenotype. In the dpn and brat brain tumor models, 29°C rearing condition revealed the tumor suppression efficiency of eag deficiency in a more aggressive tumor growth situation compare to 25°C. To study the survival of dpn brain tumor animals with or without eag deficiency, around 100 larvae or flies were analyzed for each condition. The normalized incidence of survival shown in Fig. 1c was defined as the percentage of larvae or flies of the indicated genotype over the number of control larvae of flies.

Drosophila Immunohistochemistry and Microscopy—Larval brains were dissected, fixed, and stained as previously described[19]. Briefly, 3rd instar larvae were dissected in PBS, fixed in 4% formaldehyde solution for 20 min at room temperature, and incubated with the primary antibody overnight at 4°C and secondary antibody for 2 hours at room temperature. Primary antibodies include: guinea pig anti-ase (1 5000), rabbit anti-dpn (1 500), Alexa Fluor 488 Phalloidin (Invitrogen, 1 40). Secondary antibodies conjugated to Alexa Fluor 546 or 647 (Invitrogen) were used at 1 400 or 1 100 respectively. Images were acquired with Leica SP5 confocal microscope. The brain lobe size was measured by Imaris 5.5 software after 3-D reconstruction of the z-stack of confocal images of DAPI staining. For NB quantification, type I NBs were identified by dpn^+; ase^+ labeling on the surface of brain lobe excluding optical lobe region, and type II NBs were identified by dpn^+; ase^- labeling on the dorsal region of brain lobe. For each genotype 10 brains were analyzed.

Fly brain tumor transplantation—Tissue dissections and injections were carried out as previously described[55]. Electrophysiology glass needles with a 90–100 mm opening were used. The needle tip was further sharpened into a 45-degree angle. A pressure-injection system was made by inserting the needle into a piece of silicon tubing that had a mouthpiece at the other end. Donor GFP^+, primary brain tumors or GFP^+ control brain lobes were

retrieved from 3rd instar larvae. The brain tissues or tumors were micro-dissected into small pieces. Four days old female virgin hosts were anesthetized with CO_2 and a piece of GFP$^+$ tissue was picked up with the tip of a glass needle and injected tangentially in the mid-ventral part of the abdomen. Implanted hosts were kept at 25°C and the vials were flipped every day. Tumor growth in the abdomen and metastasis into the brain were monitored for 10 days and images were taken at day 10 post transplantation. The percentage of host flies that displayed tumor growth in the abdomens or metastasis to the brains is shown in Fig. 1f. Host flies bearing transplanted tumors with *eag* loss-of-function mutation displayed significantly reduced metastasis rate compared to the host flies bearing *dpn*-overexpressing tumors (p=0.035, Student's t test). The survival of hosts was counted at daily basis until all the control flies died.

Patient Treatment

The patient is a 22 year-old male with metastatic SHH-MB. The patient was initially diagnosed in 2009 with localized MB of the posterior fossa. At the time of initial diagnosis he underwent a gross total resection followed by craniospinal irradiation therapy in combination with temozolomide. The patient was subsequently followed with serial imaging. In 2011 the patient was diagnosed with metastatic MB after complaining of localized knee pain. At that time he underwent high dose chemotherapy with cisplatin, cyclophosphamide and vincristine followed by 4 autologous stem cell transplants. That regimen was followed with 6 cycles of cis-retinoic acid and vorinostat. In 2012 the patient had further evidence of widespread metastatic disease with evidence of SHH activation by immunohistochemistry. Therefore, he was started on palliative chemotherapy with alternating cycles of celebrex, temozolomide and vismodegib. At that time the patient transferred care to UCSF with informed consent for consideration of an alternative therapy regimen. Imaging demonstrated disease progression after 7.5 months of palliative chemotherapy. His iliac tumor tested positive for EAG2 and the patient was started on thioridazine in addition to the previously described palliative chemotherapy regimen. The patient received the drug in dose escalation for approximately 2 months. His other regimen was held constant over the 2-month treatment period. Initially the patient started on 50 mg thioridazine twice daily that was subsequently increased to 150 mg in the morning and 175 mg in the evening over the course of two months. At time of initial consultation and throughout treatment period, his primary brain tumor site remained in remission. As shown in Fig. 8, his iliac tumor that tested positive for EAG2 showed evidence of treatment response most likely attributable to thioridazine as none of the other anti-tumor medications had changed prior to and between the 2-month interval PET/CTs. Given known risks of arrhythmias, tardive dyskinesias, akisthisia, hepatotoxicity and leukopenia, the patient was monitored with biweekly metabolic panels, comprehensive blood counts and EKGs in tandem with clinical visits and exams. The patient did not have adverse effects of QT prolongation or any of the above listed toxicities. However, the patient did not tolerate prolonged medication due to marked emotional lability and depression. Ultimately, despite trials of other chemotherapeutic regimens and radiation, the patient died of progressive disease 9 months later. The patient was not treated on a study protocol but per clinical recommendation by the treating physician. The patient signed informed consent to be treated with the regimen as outlined above.

Statistical Analyses

No statistical methods were used to pre-determine sample sizes and our sample sizes are similar to those used in other published studies. The statistical analyses were done afterwards without interim data analysis. Investigators were blinded to the group allocation for the thioridazine treatment experiments shown in Fig. 6c. No data points were excluded. Two-tailed Student's t-test was performed for comparison between two groups of samples. Two-Way ANOVA analyses were used to assess significance of multiple data points. The Kaplan–Meier estimator and GraphPad Prism software were used to generate survival curves. Differences between survival curves were calculated using a log-rank test. The data meet the assumptions of the tests. The variance has been tested in each group of the data and the variance is similar among genotypes. Data distribution was assumed to be normal but this was not formally tested. All data were collected and processed randomly. Each experiment has been successfully reproduced at least three times and was performed on multiple days. All data are expressed as mean ± SEM. We considered a p value less than 0.05 to be statistically significant.

A supplementary methods checklist is available.

Supplementary Material

Refer to Web version on PubMed Central for supplementary material.

Acknowledgments

References

1. Thompson MC, et al. Genomics identifies medulloblastoma subgroups that are enriched for specific genetic alterations. Journal of clinical oncology : official journal of the American Society of Clinical Oncology. 2006; 24:1924–1931. [PubMed: 16567768]

2. Kool M, et al. Integrated genomics identifies five medulloblastoma subtypes with distinct genetic profiles, pathway signatures and clinicopathological features. PLoS ONE. 2008; 3:e3088. [PubMed: 18769486]

3. Cho YJ, et al. Integrative genomic analysis of medulloblastoma identifies a molecular subgroup that drives poor clinical outcome. Journal of clinical oncology : official journal of the American Society of Clinical Oncology. 2011; 29:1424–1430. [PubMed: 21098324]

4. Northcott PA, et al. Medulloblastoma comprises four distinct molecular variants. Journal of clinical oncology : official journal of the American Society of Clinical Oncology. 2011; 29:1408–1414. [PubMed: 20823417]

5. Goodrich LV, Milenkovic L, Higgins KM, Scott MP. Altered neural cell fates and medulloblastoma in mouse patched mutants. Science (New York, NY. 1997; 277:1109–1113.

6. Yang ZJ, et al. Medulloblastoma can be initiated by deletion of Patched in lineage-restricted progenitors or stem cells. Cancer cell. 2008; 14:135–145. [PubMed: 18691548]

7. Schuller U, et al. Acquisition of granule neuron precursor identity is a critical determinant of progenitor cell competence to form Shh-induced medulloblastoma. Cancer cell. 2008; 14:123–134. [PubMed: 18691547]

8. Hatton BA, et al. The Smo/Smo model: hedgehog-induced medulloblastoma with 90% incidence and leptomeningeal spread. Cancer research. 2008; 68:1768–1776. [PubMed: 18339857]

9. Romer J, Curran T. Targeting medulloblastoma: small-molecule inhibitors of the Sonic Hedgehog pathway as potential cancer therapeutics. Cancer research. 2005; 65:4975–4978. [PubMed: 15958535]

10. Rudin CM, et al. Treatment of medulloblastoma with hedgehog pathway inhibitor GDC-0449. N Engl J Med. 2009; 361:1173–1178. [PubMed: 19726761]

11. Yauch RL, et al. Smoothened mutation confers resistance to a Hedgehog pathway inhibitor in medulloblastoma. Science (New York, NY. 2009; 326:572–574.

12. Wu X, et al. Clonal selection drives genetic divergence of metastatic medulloblastoma. Nature. 2012; 482:529–533. [PubMed: 22343890]

13. Schonherr R. Clinical relevance of ion channels for diagnosis and therapy of cancer. The Journal of membrane biology. 2005; 205:175–184. [PubMed: 16362505]

14. Pardo LA. Voltage-gated potassium channels in cell proliferation. Physiology (Bethesda). 2004; 19:285–292. [PubMed: 15381757]

15. Fraser SP, Pardo LA. Ion channels: functional expression and therapeutic potential in cancer. Colloquium on Ion Channels and Cancer. EMBO Rep. 2008; 9:512–515. [PubMed: 18451877]

16. Prevarskaya N, Skryma R, Shuba Y. Ion channels and the hallmarks of cancer. Trends Mol Med. 2010; 16:107–121. [PubMed: 20167536]

17. Huang X, Jan LY. Targeting potassium channels in cancer. The Journal of cell biology. 2014; 206:151–162. [PubMed: 25049269]

18. Homem CC, Knoblich JA. Drosophila neuroblasts: a model for stem cell biology. Development (Cambridge, England). 2012; 139:4297–4310.

19. Zhu S, et al. The bHLH repressor Deadpan regulates the self-renewal and specification of Drosophila larval neural stem cells independently of Notch. PLoS ONE. 2012; 7:e46724. [PubMed: 23056424]

20. Bowman SK, et al. The tumor suppressors Brat and Numb regulate transit-amplifying neuroblast lineages in Drosophila. Developmental cell. 2008; 14:535–546. [PubMed: 18342578]

21. Richter C, Oktaba K, Steinmann J, Muller J, Knoblich JA. The tumour suppressor L(3)mbt inhibits neuroepithelial proliferation and acts on insulator elements. Nat Cell Biol. 2011; 13:1029–1039. [PubMed: 21857667]

22. Northcott PA, et al. Multiple recurrent genetic events converge on control of histone lysine methylation in medulloblastoma. Nature genetics. 2009; 41:465–472. [PubMed: 19270706]

23. Gonzalez C. Drosophila melanogaster: a model and a tool to investigate malignancy and identify new therapeutics. Nat Rev Cancer. 2013; 13:172–183. [PubMed: 23388617]

24. Huang X, et al. Voltage-gated potassium channel EAG2 controls mitotic entry and tumor growth in medulloblastoma via regulating cell volume dynamics. Genes & development. 2012; 26:1780–1796. [PubMed: 22855790]

25. Saini N, Reichert H. Neural stem cells in Drosophila: molecular genetic mechanisms underlying normal neural proliferation and abnormal brain tumor formation. Stem Cells Int. 2012; 2012:486169. [PubMed: 22737173]

26. Reimand J, Arak T, Vilo J. g:Profiler--a web server for functional interpretation of gene lists (2011 update). Nucleic Acids Res. 2011; 39:W307–315. [PubMed: 21646343]

27. Merico D, Isserlin R, Stueker O, Emili A, Bader GD. Enrichment map: a network-based method for gene-set enrichment visualization and interpretation. PLoS One. 2010; 5:e13984. [PubMed: 21085593]

28. Bhattacharjee A, et al. Slick (Slo2.1), a rapidly-gating sodium-activated potassium channel inhibited by ATP. The Journal of neuroscience : the official journal of the Society for Neuroscience. 2003; 23:11681–11691. [PubMed: 14684870]

29. Kaczmarek LK. Slack, Slick and Sodium-Activated Potassium Channels. ISRN Neurosci. 2013; 2013

30. Hage TA, Salkoff L. Sodium-activated potassium channels are functionally coupled to persistent sodium currents. The Journal of neuroscience : the official journal of the Society for Neuroscience. 2012; 32:2714–2721. [PubMed: 22357855]

31. Rutkowski S, et al. Survival and prognostic factors of early childhood medulloblastoma: an international meta-analysis. Journal of clinical oncology : official journal of the American Society of Clinical Oncology. 2010; 28:4961–4968. [PubMed: 20940197]

32. Garcia-Ferreiro RE, et al. Mechanism of block of hEag1 K+ channels by imipramine and astemizole. The Journal of general physiology. 2004; 124:301–317. [PubMed: 15365094]

33. Herzberg IM, Trudeau MC, Robertson GA. Transfer of rapid inactivation and sensitivity to the class III antiarrhythmic drug E-4031 from HERG to M-eag channels. J Physiol. 1998; 511(Pt 1):3–14. [PubMed: 9679158]

34. Preskorn SH. Antipsychotic drug development in the pre-human-genome era: a full circle. J Psychiatr Pract. 2001; 7:209–213. [PubMed: 15990523]

35. Vanderheeren FA, Muusze RG. Plasma levels and half lives of thioridazine and some of its metabolites. I. High doses in young acute schizophrenics. Eur J Clin Pharmacol. 1977; 11:135–140. [PubMed: 320014]

36. Svendsen CN, Hrbek CC, Casendino M, Nichols RD, Bird ED. Concentration and distribution of thioridazine and metabolites in schizophrenic post-mortem brain tissue. Psychiatry Res. 1988; 23:1–10. [PubMed: 3363012]

37. Willoughby LF, et al. An in vivo large-scale chemical screening platform using Drosophila for anti-cancer drug discovery. Dis Model Mech. 2013; 6:521–529. [PubMed: 22996645]

38. Habela CW, Sontheimer H. Cytoplasmic volume condensation is an integral part of mitosis. Cell Cycle. 2007; 6:1613–1620. [PubMed: 17581282]

39. Boucrot E, Kirchhausen T. Mammalian cells change volume during mitosis. PLoS ONE. 2008; 3:e1477. [PubMed: 18213385]

40. Schwab A, Fabian A, Hanley PJ, Stock C. Role of ion channels and transporters in cell migration. Physiol Rev. 2012; 92:1865–1913. [PubMed: 23073633]

41. Jakab M, Ritter M. Cell volume regulatory ion transport in the regulation of cell migration. Contrib Nephrol. 2006; 152:161–180. [PubMed: 17065811]

42. Schwab A, Hanley P, Fabian A, Stock C. Potassium channels keep mobile cells on the go. Physiology (Bethesda). 2008; 23:212–220. [PubMed: 18697995]

43. Schwab A, et al. Polarized ion transport during migration of transformed Madin-Darby canine kidney cells. Pflugers Arch. 1995; 430:802–807. [PubMed: 7478936]

44. Schneider SW, et al. Volume dynamics in migrating epithelial cells measured with atomic force microscopy. Pflugers Arch. 2000; 439:297–303. [PubMed: 10650981]

45. Schwab A, et al. Subcellular distribution of calcium-sensitive potassium channels (IK1) in migrating cells. J Cell Physiol. 2006; 206:86–94. [PubMed: 15965951]

46. Ward RJ, et al. Multipotent CD15+ cancer stem cells in patched-1-deficient mouse medulloblastoma. Cancer research. 2009; 69:4682–4690. [PubMed: 19487286]

47. Huang X, Ketova T, Litingtung Y, Chiang C. Isolation, enrichment, and maintenance of medulloblastoma stem cells. Journal of visualized experiments : JoVE. 2010

48. Berman DM, et al. Medulloblastoma growth inhibition by hedgehog pathway blockade. Science (New York, NY. 2002; 297:1559–1561.

49. Corno D, et al. Gene signatures associated with mouse postnatal hindbrain neural stem cells and medulloblastoma cancer stem cells identify novel molecular mediators and predict human medulloblastoma molecular classification. Cancer Discov. 2012; 2:554–568. [PubMed: 22628409]

50. Lee HY, Greene LA, Mason CA, Manzini MC. Isolation and culture of post-natal mouse cerebellar granule neuron progenitor cells and neurons. Journal of visualized experiments : JoVE. 2009

51. Wallace K, Liu TH, Vaessin H. The pan-neural bHLH proteins DEADPAN and ASENSE regulate mitotic activity and cdk inhibitor dacapo expression in the Drosophila larval optic lobes. Genesis. 2000; 26:77–85. [PubMed: 10660675]

52. Wang Z, Wilson GF, Griffith LC. Calcium/calmodulin-dependent protein kinase II phosphorylates and regulates the Drosophila eag potassium channel. The Journal of biological chemistry. 2002; 277:24022–24029. [PubMed: 11980904]

53. Broughton SJ, Kitamoto T, Greenspan RJ. Excitatory and inhibitory switches for courtship in the brain of Drosophila melanogaster. Current biology : CB. 2004; 14:538–547. [PubMed: 15062094]

54. Vahasoyrinki M, Niven JE, Hardie RC, Weckstrom M, Juusola M. Robustness of neural coding in Drosophila photoreceptors in the absence of slow delayed rectifier K+ channels. The Journal of neuroscience : the official journal of the Society for Neuroscience. 2006; 26:2652–2660. [PubMed: 16525044]

55. Janic A, Mendizabal L, Llamazares S, Rossell D, Gonzalez C. Ectopic expression of germline genes drives malignant brain tumor growth in Drosophila. Science (New York, N Y. 2010; 330:1824–1827.
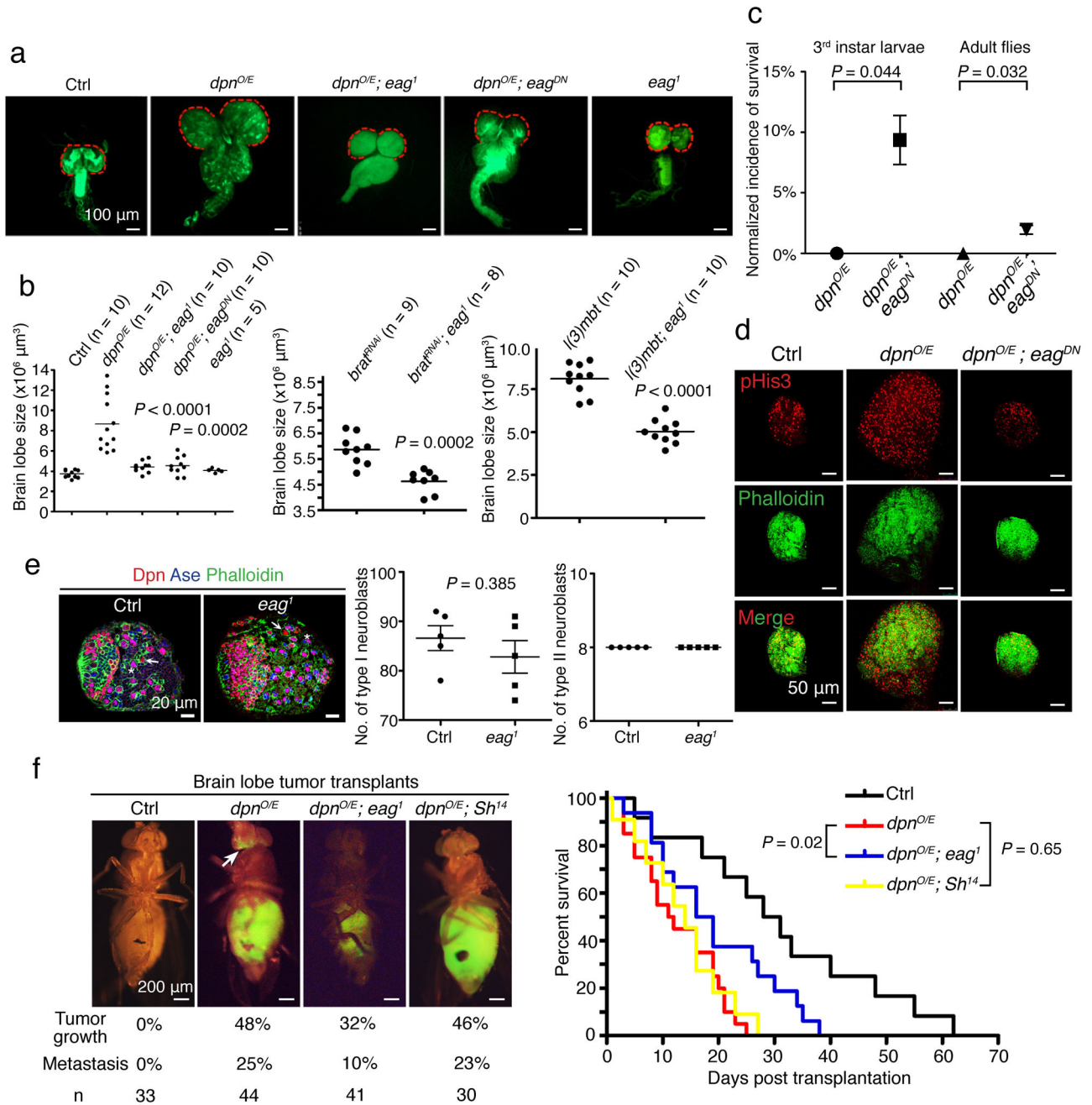
Figure 1. *Drosophila* Eag channel deficiency reduces brain tumor growth and metastasis

a, *insc-Gal4*-driven *dpn* overexpression in the neuroblast lineage leads to tumor growth in brain lobes (red dash lines) and the ventral nerve cord of 3rd instar larvae. *eag* mutation (*eag¹* or *eag^DN*) reduces the size of tumor-bearing brain lobes. **b**, *eag* mutation decreases the volume of brain lobes bearing tumors induced by *dpn* overexpression, *brat* knockdown, and *l(3)mbt* loss-of-function (two-tailed Student's t-test). **c**, *eag* mutation increases the survival rate of brain tumor-bearing 3rd instar larvae raised at 29°C and adult flies raised at 25°C (n = 95 and 105 for *dpn^O/E* and *dpn^O/E; eag^DN* larvae, respectively; n = 88 and 100 for *dpn^O/E* and *dpn^O/E; eag^DN* adults, respectively; two-tailed Student's t-test). **d**, *eag* mutation reduces

proliferation in *dpn*-overexpressing brain lobe tumors. **e**, Control 3rd instar larvae and larvae with *eag* loss-of-function have comparable numbers of type I and type II neuroblasts per brain lobe (n = 10 brain lobes for each genotype, two-tailed Student's t-test). **f**, The metastatic potential of brain lobe tumor cells in transplantation assay as well as lethality of host flies is reduced by *eag* loss-of-function, but not by mutation of another potassium channel gene *Shaker* (Sh^{14}) (n = 12, 20, 16 and 11 for control, *$dpn^{O/E}$, $dpn^{O/E}$; eag^1* and *$dpn^{O/E}$; Sh^{14}*, respectively, log-rank Kaplan-Meier test). Error bars show ± SEM.
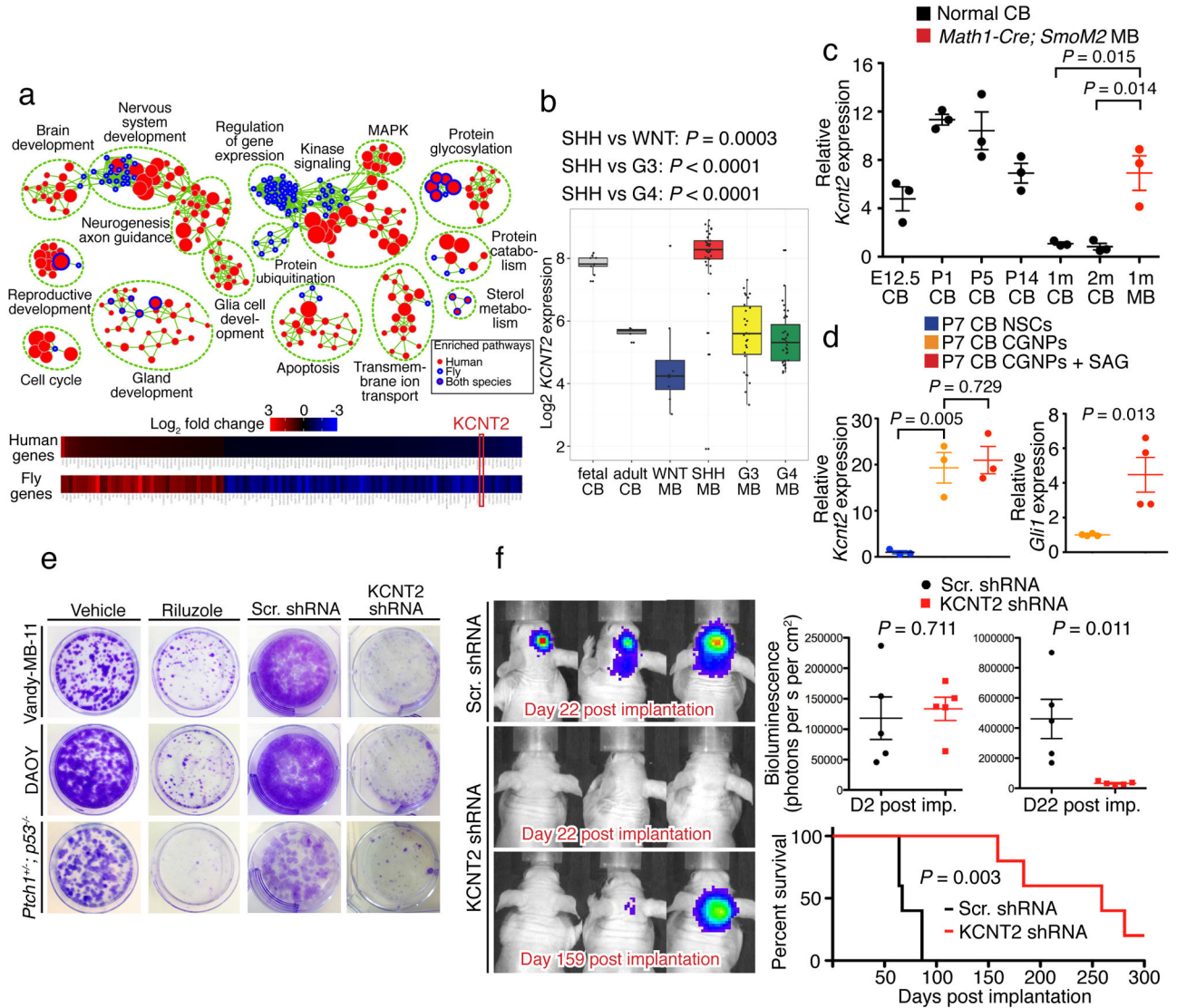
Figure 2. Cross-species transcriptomic studies identify KCNT2 as a novel potassium channel that is enriched in SHH-MB and regulates tumor growth

a, Top: Enrichment map of conserved pathways transcriptionally altered upon genetic suppression of EAG2 in human MB (nodes with red cores) and *eag* in fly brain tumor (nodes with blue rims). Bottom: *KCNT2* is the only ion channel-encoding gene among the 120 commonly affected orthologous gene pairs in human and fly. **b**, *KCNT2* expression is higher in human fetal than adult cerebella, and elevated in SHH-MB compared to other MB subgroups (one-tailed Mann-Whitney U test). **c**, Mouse *Kcnt2* expression is higher in embryonic (E12.5) and early postnatal (P1, P5 and P14) cerebella than young (1 month and 2 months old) adult cerebella. *Math1-Cre; SmoM2* Shh-MB tumors demonstrate significant *Kcnt2* overexpression (n = 3 brains for each group, two-tailed Student's t-test). **d**, Cerebellar CGNPs display higher *Eag2* expression compared to NSCs, while treating CGNPs with SAG increases the expression of the Shh pathway readout *Gli1* without affecting *Eag2* (n = 3 or 4 independent cultures and qPCR experiments, two-tailed Student's t-test). Error bars

show ± SEM. **e**, Treating MB cells with 20 μM riluzole, a persistent sodium current blocker, or shRNA targeting KCNT2 reduces clonogenic growth. **f**, KCNT2 knockdown inhibits intracranial MB tumor growth and enhances mouse survival (n = 5 for each group, two-tailed Student's t-test for bioluminescence comparison, log-rank Kaplan-Meier test for survival comparison).
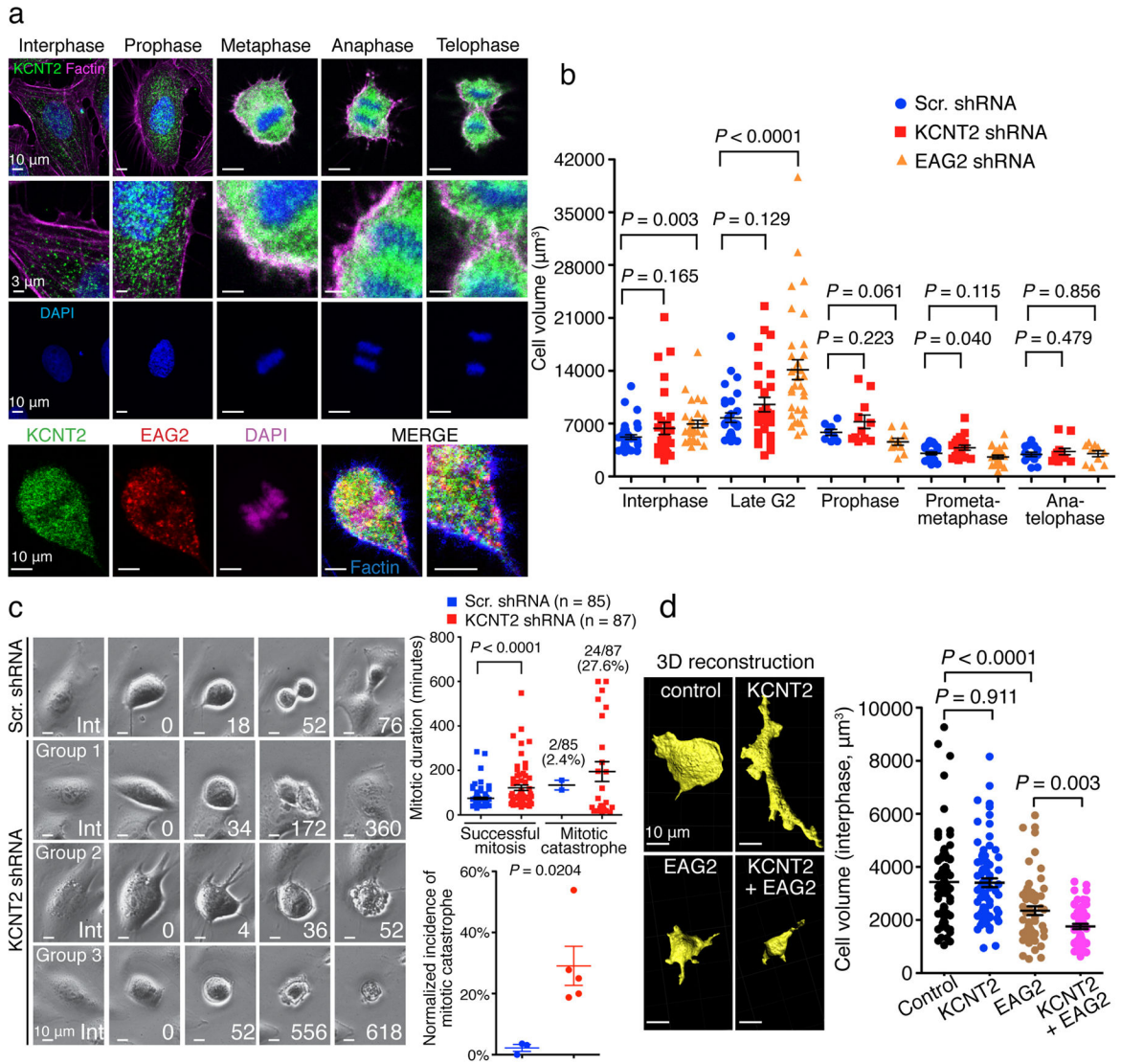
Figure 3. KCNT2 and EAG2 functionally cooperate to regulate mitotic cell volume

a, Top: KCNT2 channel enriches to MB cell membrane from metaphase through telophase. Bottom: KCNT2 and EAG2 channels exhibit largely non-overlapping localization within MB cells. **b**, EAG2-deficient MB cells display increased cell volume at interphase and late G2 phase, whereas KCNT2-deficient MB cells exhibit cell volume increase at prometaphase and metaphase (n = 36, 29, 8, 25 and 14 cells for Scr. shRNA, n = 32, 28, 11, 19 and 12 cells for KCNT2 shRNA, n = 29, 33, 10, 24 and 10 cells for EAG2 shRNA at interphase, late G2, prophase, prometaphase/metaphase and anaphase, respectively, two-tailed Student's t-test). **c**, Time-lapse imaging of KCNT2-deficient MB cells revealing abnormally prolonged mitosis (Group 1), mitotic catastrophe soon after entering mitosis (Group 2), or long mitotic arrest (Group 3), leading to longer mitotic duration and higher incidences of mitotic catastrophe (two-tailed Student's t-test). **d**, Overexpression of EAG2 and KCNT2 reduces COS7 cell volume to a greater extent than overexpression of EAG2, whereas overexpression of KCNT2 channel markedly changed COS7 cell morphology without reducing the overall
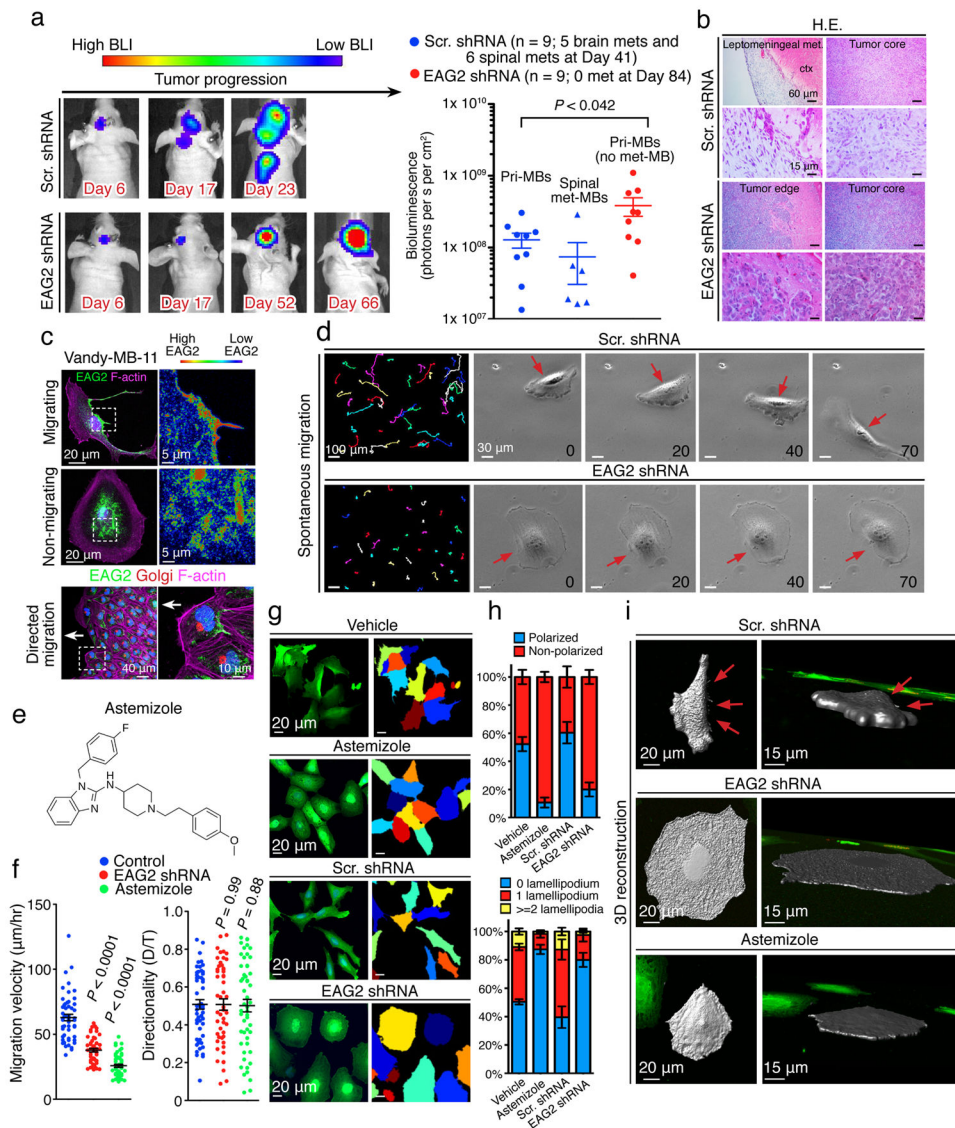
cell volume (n = 79, 76, 57 and 54 for GFP, KCNT2, EAG2 and KCNT2 + EAG2, respectively, two-tailed Student's t-test). Error bars show ± SEM.

Figure 4. EAG2 channel promotes MB metastasis and enriches to the trailing edge to regulate MB cell motility

a, Longitudinal bioluminescence imaging reveals intracranial and spinal cord metastasis of control Vandy-MB-11 tumor but not EAG2-deficient tumor (n = 9 for each group, two-tailed Student's t-test). **b**, Histological examination reveals no leptomeningeal spread of Vandy-MB-11 tumors with EAG2 knockdown. **c**, EAG2 enrichment to the cell rear and trailing edge of Vandy-MB-11 (passage 2) MB cells during migration. **d**, EAG2 knockdown hampers spontaneous MB cell migration. Left: migratory routes of Vandy-MB-11 cells over 5 hours. Right: representative images over 70 minutes show loss of cell rear contraction (red arrows) due to EAG2 knockdown. **e**. Chemical structure of astemizole. **f**, EAG2 knockdown or astemizole treatment reduces MB cell migratory velocity (μm/hour) but not directionality (D/T, distance/time) (n = 52 for each group, two-tailed Student's t-test). **g**, Defective migratory polarization and rounded morphology of Vandy-MB-11 cells with EAG2 knockdown or astemizole treatment, as revealed by cytoplasmic GFP and indicated by

pseudocolors. **h**, Reduced lamellipodia and migratory polarization 4–5 days after infecting Vandy-MB-11 cells with lentivirus expressing EAG2 shRNA or 2 days after incubating MB cells with 5 μM astemizole (n = 382, 325, 164 and 127 randomly selected cells for vehicle, astemizole, Scr. shRNA and EAG2 shRNA respectively). **i**, 3-D reconstruction of Vandy-MB-11 cells with EAG2 knockdown or channel inhibition by astemizole revealing loss of fan-shaped leading edge and retraction fibers at the trailing edge (red arrows). Error bars show ± SEM.
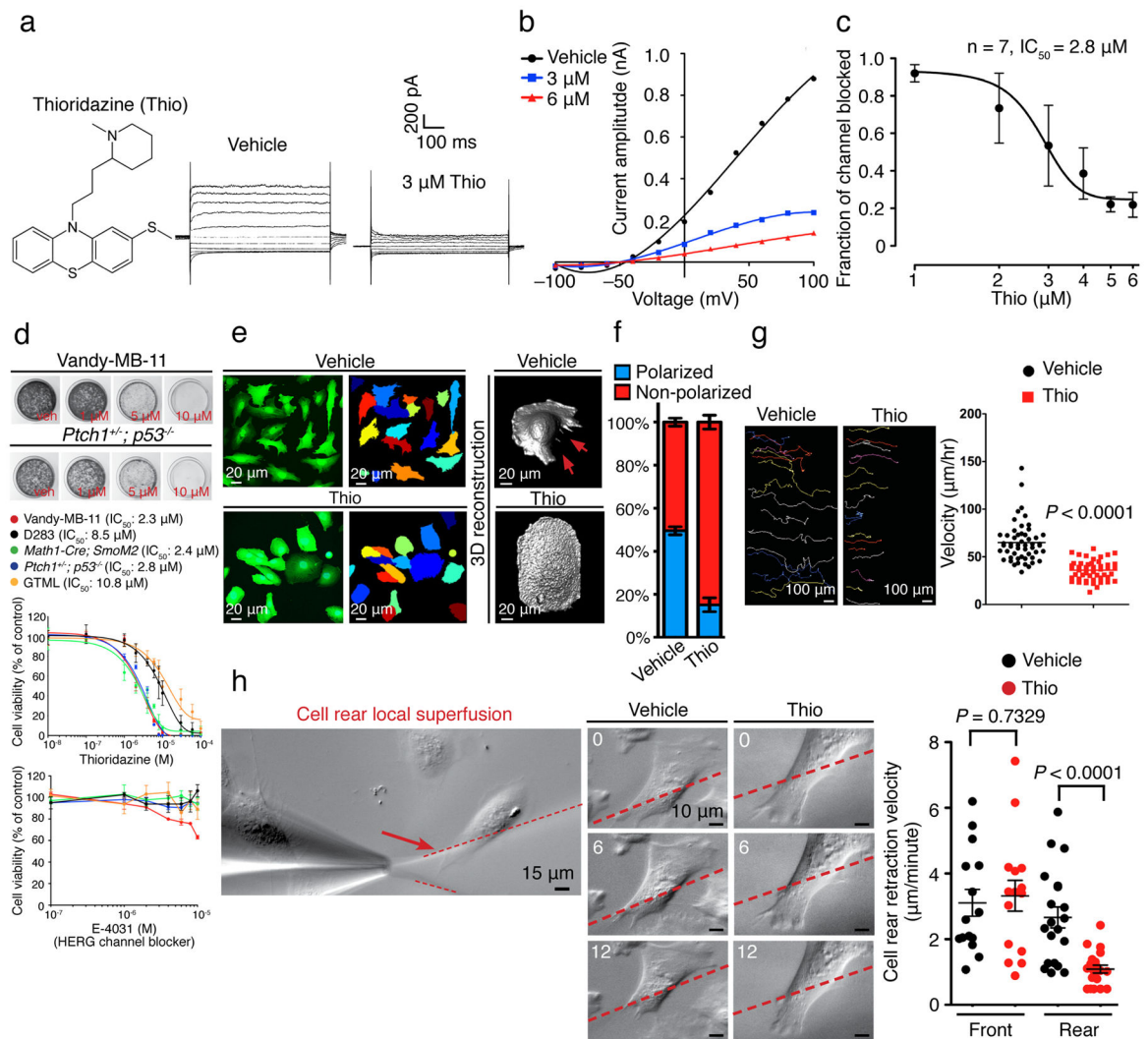
Figure 5. Thioridazine is a novel EAG2 blocker that reduces MB cell viability and mobility
(**a–c**) With a chemical structure distinct from that of astemizole, Thioridazine blocks EAG2-conducted outward potassium current, as shown in representative traces (**a**), I–V curves (**b**) and dose-response curve (**c**). **d**, Thioridazine, but not E-4031, reduces MB cell growth. (**e–g**) Thioridazine treatment (5 μM) of Vandy-MB-11 cells leads to rounded morphology and loss of cell rear contraction (red arrows) (**e**), impaired migratory polarization (**f**) (n = 260 and 340 for vehicle and Thio group, respectively, of randomly selected cells quantified for each condition), and reduced cell motility as revealed by the colored migratory routes (left to right) of individual Vandy-MB-11 cells over 16 hours shown on the left, with quantifications shown on the right (n = 52 and 48 for vehicle and Thio group, respectively, two-tailed Student's t-test) (**g**). **h**, The velocity for rear retraction was significantly reduced by local superfusion of thioridazine to the rear, but not the front end, of Vandy-MB-11 cells. Representative images of cell rear retraction with local vehicle and thioridazine application over 12 minutes are shown (n = 15 and 20 for the "front" and "rear" groups, respectively, two-tailed Student's t-test). Error bars show ± SEM.
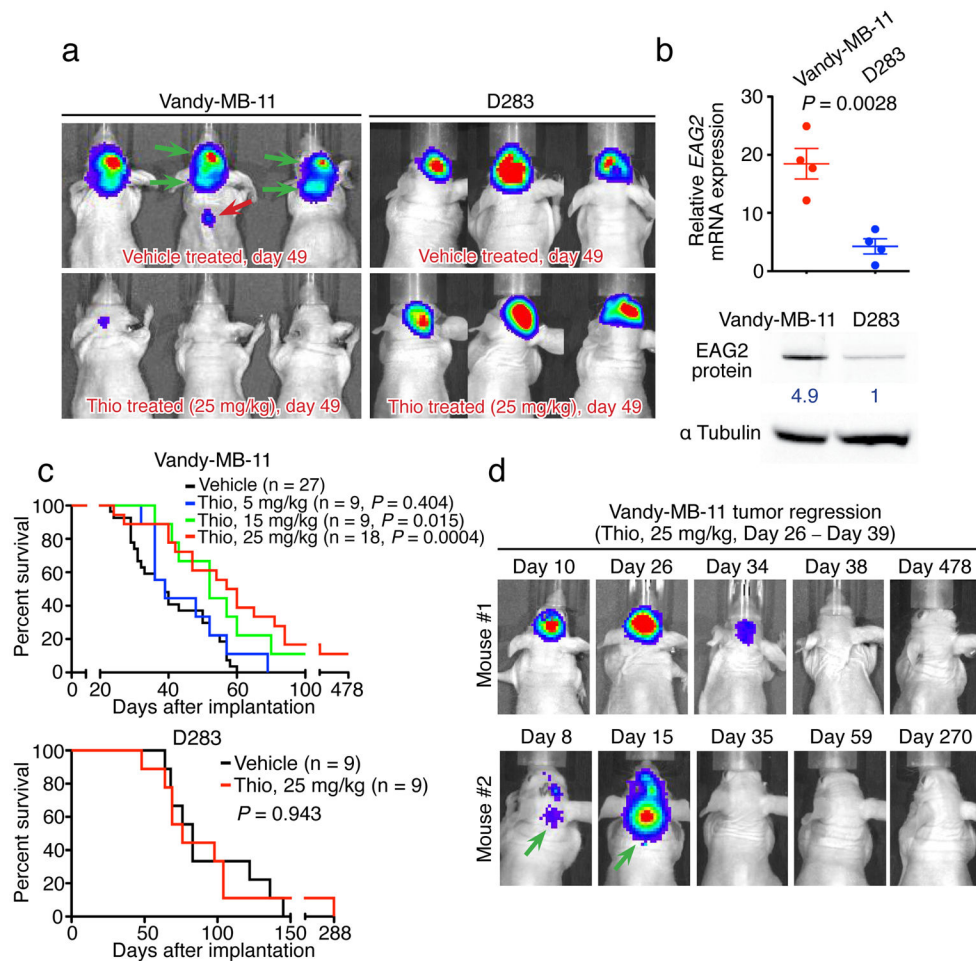
Figure 6. Thioridazine inhibition of EAG2 channel reduces intracranial MB growth and metastasis

a, Daily intraperitoneal injection of thioridazine for two weeks reduces intracranial tumor burden and inhibits brain and spinal cord metastasis of Vandy-MB-11 but not D283 tumors. **b**, High *EAG2* expression in Vandy-MB-11 but not D283 cells (n = 4 independent cultures and qPCR experiments, two-tailed Student's t-test). Full-length Western blot images are presented in Supplementary Fig. 9. **c**, Thioridazine treatment (at 15 mg/kg and 25 mg/kg) significantly enhances the survival of mice bearing Vandy-MB-11 but not D283 tumors (log-rank Kaplan-Meier test). **d**, Longitudinal bioluminescence imaging revealed complete and sustained regression of Vandy-MB-11 tumor growth in two mice treated with 25 mg/kg thioridazine from Day 26 to Day 39. Green arrows indicate metastasis before treatment. Error bars show ± SEM.
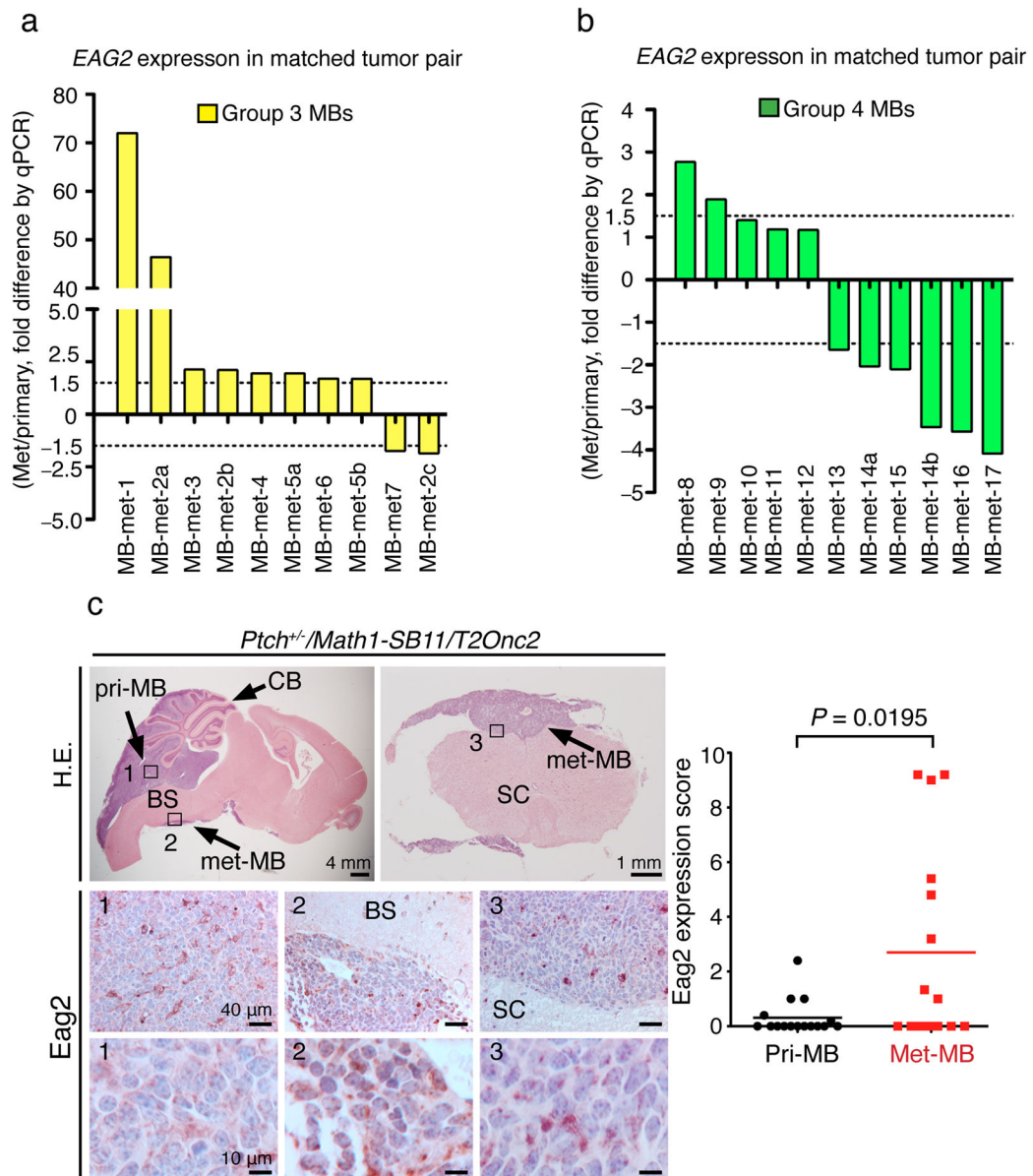
Figure 7. A subset of metastasized MB tumors display EAG2 upregulation compared to matched primary tumors

a, qPCR analysis shows that 80% (8/10) of metastasized human MBs (met-MBs) display >1.5 fold increase of *EAG2* transcript compared to matched primary MBs, in 86% (6/7) group 3 patients (patient 2 has three metastases, met-MB-2a, 2b and 2c, and patient 5 has two metastases, met-MB-5a and 5b). **b**, qPCR analysis shows 18% (2/11) of the met-MBs with >1.5 fold *EAG2* upregulation in 20% (2/10) of the group 4 patients (patient 14 has two metastases, met-MB-14a and 14b). **c**, Immunohistochemical analysis of the *Ptch*^{+/−}*/Math1-SB11/T2Onc2* mouse model of Shh-MB shows that 37.5% (6/16 of the matched tumor pairs) of metastasized tumors display elevated Eag2 protein expression (n = 16 matched primary and met-MB pairs, two-tailed paired Student's t-test). CB: cerebellum; BS: brainstem; SC: spinal cord. Error bars show ± SEM.
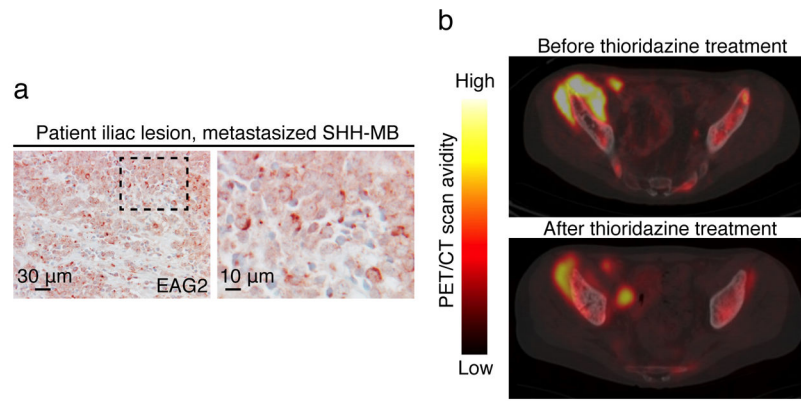
Figure 8. A case report of thioridazine treatment of a patient with metastatic SHH-MB
a, Patient biopsies at the metastasized iliac lesion show prominent *EAG2* expression. **b**, PET-CT scans before and after thioridazine treatment show reduction of tumor volume and 2-deoxyglucose avidity.